Industrial Chemistry & Materials

工业化学与材料(英文)

Volume 1
Number 1
February 2023
Pages 1-148

REVIEW ARTICLE
Jiandong Pang, Xian-He Bu *et al.*
Recent progress in metal–organic frameworks (MOFs) for electrocatalysis

ISSN 2755-2500 (Online)
ISSN 2755-2608 (Print)

rsc.li/icm

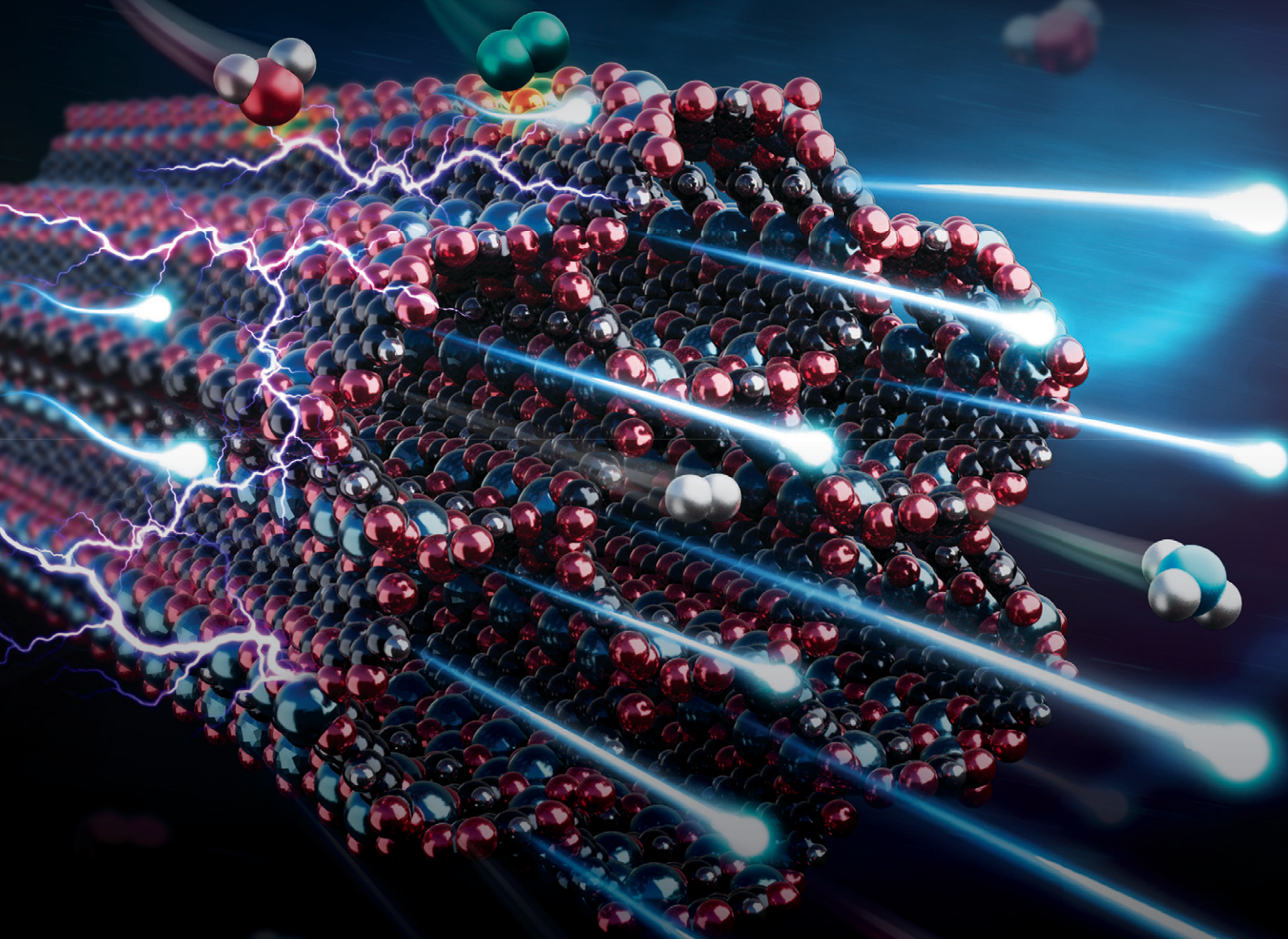

ROYAL SOCIETY OF CHEMISTRY

ICM Industrial Chemistry & Materials

Industrial Chemistry & Materials

ROYAL SOCIETY OF CHEMISTRY

REVIEW

View Article Online
View Journal | View Issue

Cite this: *Ind. Chem. Mater.*, 2023, **1**, 9

Recent progress in metal–organic frameworks (MOFs) for electrocatalysis

Cha Li,[a] Hao Zhang,[a] Ming Liu,[a] Fei-Fan Lang,[a] Jiandong Pang *[ab] and Xian-He Bu *[abc]

Electrocatalytic technology opens a new path to solve the existing problems in fossil fuel consumption and environmental pollution as well as efficient energy use. Metal–organic frameworks (MOFs), a class of crystalline porous materials with high specific surface area, high porosity and customizable structures, have emerged as promising electrocatalysts. However, their inherently low electrical conductivity and stability greatly hinder their further applications. Therefore, strategies such as synthesizing two-dimensional conductive MOFs, designing unsaturated metal sites, and building MOF nanoarrays have been developed to enhance the conductivity and catalytic reaction transfer rates of MOFs, accompanied by the rational designs of MOFs for improving their stability. In this review, the applications of MOF-based electrocatalysts in the hydrogen evolution reaction (HER), hydrogen oxidation reaction (HOR), oxygen evolution reaction (OER), oxygen reduction reaction (ORR) and nitrogen reduction reaction (NRR) are presented in detail with the classification of monometallic MOFs, bimetallic MOFs, MOF-based composites and MOFs as supports. In addition, the relationship between the structure and performance is discussed through DFT calculations used in related work. Finally, future challenges and application prospects of MOFs in electrocatalysis are highlighted.

Received 26th December 2022,
Accepted 24th January 2023

DOI: 10.1039/d2im00063f

rsc.li/icm

Keywords: Metal–organic frameworks; Electrocatalyst; Catalytic performance; Catalysis; Energy conversion.

1 Introduction

Energy and the environment have always been hot topics of concern to countries around the world and are the basis of national economic and social development.[1] In recent years, with the rapid development of the economy, energy shortage and environmental pollution problems have become more and more serious. There is an increasing need to develop sustainable and efficient clean energy to promote a new energy revolution.[2,3] Electrocatalysis, an efficient and clean chemical energy conversion process, has the ability to convert molecules with high atmospheric content (*e.g.* oxygen, nitrogen and carbon dioxide) and water into products that are beneficial to humans (*e.g.* oxygenated compounds, ammonia, hydrocarbons and hydrogen).[4] Electrocatalysts play a crucial role in electrocatalytic processes because they reduce the activation energy of electrocatalytic reactions and provide conduction sites for electrochemical reactions, thus improving the rate and selectivity of the reactions. However, electrocatalysts for various types of electrocatalytic reactions (hydrogen evolution reaction, hydrogen oxidation reaction, oxygen reduction reaction, oxygen evolution reaction, and nitrogen reduction reaction) are currently some distance away from commercial applications due to the limitations of expensive and scarce resources of precious metals and the poor activity, selectivity, and stability of non-precious metal

[a] *School of Materials Science and Engineering, Smart Sensing Interdisciplinary Science Centre, National Institute for Advanced Materials, TKL of Metal and Molecule-Based Material Chemistry, Nankai University, Tianjin 300350, P. R. China. E-mail: jdpang@nankai.edu.cn, buxh@nankai.edu.cn*
[b] *Haihe Laboratory of Sustainable Chemical Transformations, Tianjin, 300192, P.R. China*
[c] *State Key Laboratory of Elemento-Organic Chemistry, College of Chemistry, Nankai University, Tianjin 300071, P. R. China*

Cha Li

Cha Li received his M.S. degree from Tianjin Normal University in 2022. He is currently a PhD student at Nankai University under the supervision of Professor Jiandong Pang and Professor Xian-He Bu. His current research focuses on the applications of crystalline porous materials in energy catalysis and functional devices.

catalysts. Therefore, it is crucial to develop advanced electrocatalysts with high catalytic performance to cross this gap.

Coordination polymers are compounds formed by the assembly of metal ions or metal clusters with organic ligands through coordination bonds.[5,6] The more prominent of these are porous coordination polymers with pore structures. Porous coordination polymers formed from ligands with metal ions/metal clusters are commonly referred to as metal–organic frameworks.[7] Since the concept of metal–organic frameworks (MOFs) was first introduced by Yaghi in 1995,[8] a large number of MOFs have been reported in the last three decades.[9–14] MOFs have attracted extensive interest and in-depth research from chemical and materials scientists and have been widely used in gas adsorption/separation, catalysis, sensing, and drug delivery due to the following main advantages: high crystallinity, large porosity and surface area, structural diversity and designability.[15–20]

Meanwhile, MOFs have been applied to different types of electrocatalytic reactions in different presence modes and have obtained impressive catalytic activities. These include the hydrogen evolution reaction (HER), hydrogen oxidation reaction (HOR), oxygen reduction reaction (ORR) and oxygen evolution reaction (OER). These reactions are the core reactions of the following devices or cells: metal–air cells, renewable fuel cells, electrolytic water to hydrogen devices and other important electrochemical energy conversion devices. The electrocatalytic nitrogen reduction reaction to ammonia also shows attractive application prospects in the field of energy conversion. Several research groups have reviewed the progress of MOF-based catalysts for the electrocatalytic HER, OER and ORR.[21–27] However, the recent advances in MOF-based electrocatalytic HOR and NRR processes have rarely been summarized. Meanwhile, with the continuous development, plentiful MOF electrocatalysts have appeared recently. Hence it is necessary to summarize the literature reports in a timely manner, which is helpful for researchers to design MOF-based electrocatalysts accurately and deepen the understanding of the relevant reaction mechanisms.

Here, we intend to summarize the progress of MOFs in various electrocatalytic reactions, including the HER, HOR, OER, ORR and NRR. The focus is on the design of MOF materials, the solution to key problems in catalytic reactions, structure–property relationships, catalytic performance and mechanisms. First, we list the evaluation parameters for assessing various types of electrocatalytic reactions. Then, we systematically summarize the research progress of MOF-based electrocatalysts in recent years by classifying monometallic MOFs, bimetallic MOFs, MOF-based composites, and MOFs as supports, and initiate an in-depth discussion through the reported reaction processes, reaction mechanisms, and modelling theory calculations involved. Among them, we intersperse the progress to cover the design strategies of general MOF-based catalysts used to improve the activity, conductivity and stability of electrocatalytic reactions, including the synthesis of two-dimensional conducting MOFs, the design of unsaturated metal sites, the construction of MOF nanoarrays and the selection of highly stable MOFs. Finally, we provide an outlook on the future opportunities and challenges for MOF-based electrocatalysis and present the prospects for future research.

2 Electrocatalytic performance evaluation and measurement

In order to assess the performance of the above-mentioned electrocatalytic reactions precisely, the following parameters for the evaluation of important reactions are summarized in this section.

Jiandong Pang

Jiandong Pang is now a professor at the School of Materials Science and Engineering of Nankai University. He received his Ph.D. degree in Chemistry (2016) under the supervision of Professor Maochun Hong from Fujian Institute of Research on the Structure of Matter, Chinese Academy of Sciences. He then joined Professor Hong-Cai Zhou's group in the same year as a postdoctoral research associate at TAMU. His current research interests focus on the design and synthesis of ultrastable crystalline porous materials with intriguing structures and potential functions in gas adsorption and separation, fluorescence, catalysis, and recognition.

Xian-He Bu

Xian-He Bu is an academician of the Chinese Academy of Sciences. He is a full-time professor at Nankai University and serves as the director of Tianjin Key Lab of Metal and Molecule-Based Material Chemistry. His research interests include functional coordination chemistry, crystal engineering, molecular magnetism, and material chemistry.

2.1 Cyclic voltammetric curves (CV) and linear polarization curves (LSV)

Cyclic voltammetric curves (CV) and linear polarization curves (LSV) are the most intuitive methods to evaluate the activity of electrocatalysts. Generally, the system is saturated with high purity hydrogen (for the HER)/high purity nitrogen (for the NRR)/high purity oxygen (for the ORR)/high purity argon (for the HER and OER) before the test. The system is then subjected to a continuous CV scan to activate the catalyst to reach a steady state, followed by an LSV test to obtain a linear scan voltammetric curve. Different information can be obtained from the LSV curves for different electrocatalytic reactions, such as overpotential, onset potential, half-wave potential, *etc.*

2.2 Tafel curve

The Tafel curve describes the dependence between the steady-state current density and the individual overpotentials. Typically, the logarithm of the current density and the overpotential of the catalyst have a linear correlation. The specific Tafel equation is $\eta = a + b\log j$ (η is the overpotential, j is the current density, and b is the Tafel slope), where the Tafel slope (b) and the exchange current density (j_0) are two important kinetic parameters to evaluate the catalyst performance. The magnitude of the Tafel slope can reflect the catalytic mechanism and reaction kinetics of the catalytic reaction process. The exchange current density (j_0) is the current density when the overpotential of the catalyst is zero, which reflects the intrinsic catalytic capacity of the electrode material at equilibrium potential. In general, high-performance electrocatalysts have both a low Tafel slope (b) and a high exchange current density (j_0).

2.3 Koutecky–Levich plot

For the hydrogen oxidation and oxygen reduction reactions, the relationship between the magnitude of the total current density (j) of the electroactive species and the electrode rotational velocity (ω) in the region jointly controlled by diffusion and reaction kinetics in the rotating disk electrode (RDE) process is known as the Koutecky–Levich equation:

$$\frac{1}{j} = \frac{1}{j_k} + \frac{1}{j_L} = \frac{1}{nFkC_0} + \frac{1}{0.62nFC_0(D_0)^{2/3}v^{-1/6}\omega^{1/2}}$$

where j_k is the kinetic current density, j_L is the diffusion current density, n is the number of electrons transferred, F is the Faraday constant, k is the electron transfer rate constant, D_0 is the diffusivity of H_2/O_2, v is the kinematic viscosity, C_0 is the solubility of H_2/O_2 in the electrolyte and ω is the rotational speed. The K–L equation is based on the laminar fluid dynamics of a smooth electrode surface. Therefore, as-prepared catalyst films during the test must be as thin, uniform and smooth as possible, and the amount of catalyst added must be strictly controlled to ensure the accuracy of the calculated kinetic currents. The electron transfer number (n), the rate constant (k) and the kinetic current density are the key parameters that can be calculated from the K–L equation.

2.4 Electrochemically active surface area (ECSA)

The electrochemically active surface area is the active area of the catalyst that is actually involved in the reaction during the electrocatalytic reaction and is a concept relative to the geometric area. It is not scientific to compare the performance of different catalysts based only on the unit geometric area of the electrode. This is because different catalysts have different catalyst loading substrate roughness. Therefore, the concept of electrochemically active surface area is introduced and used as a benchmark to compare the catalytic performance of different catalysts. The value of the differential capacitance (C_{dl}) is generally measured by cyclic voltammetry and impedance spectroscopy to obtain the electrochemically active surface area of the catalyst.

2.5 Turnover frequency (TOF)

The turnover frequency (TOF) indicates the number of converted reactant molecules into target products per catalyst active site per unit time, showing the intrinsic catalytic activity of a catalytically active site. It is difficult to obtain the conversion frequency of heterogeneous catalysts, mainly because the number of active sites actually participating in the reaction is difficult to define.

2.6 Faraday efficiency (FE)

The Faraday efficiency is a common metric for electrocatalytic systems and describes the utilization of electrons in a particular electrocatalytic reaction process. For a particular electrocatalytic reaction, it is generally the ratio between the actual target product amount and the theoretical target product amount. It can be tested using drainage methods, oxygen sensors, gas chromatographs, *etc.*

2.7 Ammonia yield rate

For ammonia production by electrocatalytic nitrogen reduction, the ammonia yield rate is critical and refers to the amount of nitrogen to ammonia conversion achieved under a nitrogen atmosphere. The ammonia content can be tested with a UV spectrophotometer using Nessler's reagent, indophenol blue, nitrogen 15 gas labeling, ion chromatography, *etc.*

2.8 Stability

For each electrocatalytic reaction, the stability of the catalyst is as critical as the catalytic activity of the catalyst to achieve further commercial applications. The stability of a catalyst is not only related to the structural and compositional stability of the catalyst itself, but also to the preparation process of the electrode. There are several types of stability tests: one is to test the potential *versus* time curve (I–t curve or V–t curve)

at a certain current density; another is to test the current *versus* time at a constant overpotential; the other is to perform successive CV tests on the catalyst in the potential interval corresponding to the electrocatalytic reaction and assess the stability of the catalyst by comparing the change in the potential and current density between the first CV curve and the last CV curve. In addition, for the hydrogen oxidation reaction, the tolerance to carbon monoxide needs to be evaluated.

There are many key factors affecting the electrocatalytic performance, external factors including the temperature, pressure, operating environment and errors, *etc.*, and internal factors including the structure and composition of the catalyst, the choice of the substrate electrode carrier of the catalyst, the defects on the catalyst surface, the form of hybridization and the active species of the morphological catalyst. Therefore, in the process of electrocatalytic experimental testing, the external factors such as the temperature, humidity and pressure of the environment need to be controlled and unified. Moreover, different reference electrodes are selected according to different acidic and alkaline environments. For example, when the electrolyte is alkaline, the Hg/HgO electrode (E(RHE) = E(Hg/HgO) + 0.0591 × pH + 0.098) should be selected as the reference electrode. When the electrolyte is neutral, it is recommended to select the saturated calomel electrode (E(RHE) = E(SCE) + 0.0591 × pH + 0.244) or the Ag/AgCl electrode (E(RHE) = E(Ag/AgCl) + 0.0591 × pH + 0.197) as the reference electrode. For acid electrolytes, the saturated calomel electrode or the Hg/Hg_2SO_4 electrode (E(RHE) = E(Hg/Hg_2SO_4) + 0.0591 × pH + 0.656) should be selected as the reference electrode. For uniform comparison, they are generally converted to the reversible hydrogen electrode (RHE).

3 MOF-based electrocatalysts for the hydrogen evolution reaction

As fossil fuels continue to be depleted, it is critical to develop clean and sustainable energy sources.[28] Hydrogen (H_2) is a clean, carbon-free energy carrier and a promising alternative for solving energy supply problems in the future.[29,30] The rational and efficient use of hydrogen energy is one of the most pressing issues today. Continuous production of high-purity hydrogen by electrochemical water splitting is a particularly attractive route, but requires efficient and stable electrocatalysts to drive the hydrogen evolution reaction (HER) and oxygen evolution reaction (OER) in the water splitting process.[31] To date, platinum-based electrocatalysts remain the benchmark catalysts for the HER due to their ultrafast kinetics as well as low overpotential, but their high price and scarce resources limit their large-scale application, thus prompting the search for efficient and stable HER electrocatalysts.[32] The electrocatalytic reaction occurs between the solid–liquid interface of the electrode and the electrolyte, and there are different reaction processes and different reaction mechanisms in each of the acid–base electrolytes. The reaction processes of the hydrogen evolution reaction in acidic and basic electrolytes are as follows,[33] respectively.

Acidic:

$$\text{Volmer step: } H^+ + e^- \rightarrow H^*$$

$$\text{Heyrovsky step: } H^+ + H^* + e^- \rightarrow H_2$$

$$\text{Tafel step: } 2H^* \rightarrow H_2$$

Alkaline:

$$\text{Volmer step: } H_2O + e^- \rightarrow OH^- + H^*$$

$$\text{Heyrovsky step: } H_2O + H^* + e^- \rightarrow OH^- + H_2$$

$$\text{Tafel step: } 2H^* \rightarrow H_2$$

The present hydrogen evolution reaction can be divided into three primitive reactions. As an example of the hydrogen evolution reaction in an alkaline medium: first, hydrated protons adsorb onto the catalyst (*) surface and get an electron, and a reduction reaction takes place to form adsorbed H* and OH^-. This process is called the electrochemical step (Volmer step). Then, the adsorbed H (H*) can form H_2 in two ways. One is the electrochemical desorption step (Heyrovsky step), where H* binds to the hydrated proton in solution and gets an electron from the catalyst surface to form H_2. The other is the complex desorption step (Tafel step), where two H* combine directly to form H_2.

The reason why the HER is more favorable under acidic conditions is that the energy required for the adsorption of hydrated protons (H_3O^+) in the Volmer step of the HER under acidic conditions is much less than that required to break the H–O–H bond of the water molecule under alkaline conditions.[34] Also, the Volmer step is required for both acid and alkaline media. Meanwhile, according to the above reaction equations, both Volmer–Heyrovsky and Volmer–Tafel pathways involve the formation of intermediate H*. Therefore, the free energy change of H adsorption (ΔG_{H^*}) is an important indicator for predicting/estimating the activity of HER catalysts.[35] ΔG_{H^*} is highly dependent on the electronic structure and the intrinsic surface chemistry of the material. In general, according to the Butler–Volmer equation and Sabatier's principle, the hydrogen adsorption energy (HBE) of an ideal electrocatalyst should not be too high nor too low, that is, with an optimal HBE.[36] Therefore, it is desirable to have a near-zero ΔG_{H^*} in the design of the electrocatalyst.

Metal–organic frameworks have the advantages of uniform pore size distribution, abundant porous structure and high specific surface area. Therefore, the synthesis of MOFs with predictable structures and high stability has been an important goal in the field of metal–organic framework research. A clear strategy to guide the design of ligands and metals will help to develop novel functionalized MOFs and provide a fire-new reference for various fields. Synthesis with the same reactants may lead to MOFs with different topologies and properties, and the reaction time, method and temperature of synthesis will also affect the crystal structure, morphology and pore environment of MOFs, which further affect the performance of the materials. There are two common adjustment directions for the synthesis of MOF-based electrocatalysts, *i.e.*, tuning the size of MOFs and modulating the conductivity of MOFs. For regulating the size of MOFs, specific synthesis methods include chemical/physical exfoliation, solvothermal, hydrothermal, surfactant-assisted, microwave heating, ultrasonic, and electrochemical *in situ* synthesis methods to make the MOFs possess nanoscale size, which can maximize the exposure of catalytically active sites while accelerating the electron transport; for improving the conductivity of MOFs, specific synthesis methods include *in situ* growth of MOFs on conducting substrates, self-assembly methods, *etc.* Furthermore, based on the diversity of metal ions and ligands, specific metal centers and ligands containing specific organic functional groups can be selected to design and synthesize MOFs with high stability under a catalytic environment and applied to the study of electrocatalysis. To make MOFs with high stability, researchers generally choose to construct frameworks using carboxylate-based ligands (hard Lewis bases) and high-valent metal ions (hard Lewis acids, such as Al^{3+}, Cr^{3+}, Fe^{3+}, Ti^{4+}, and Zr^{4+}) or azo-based ligands (soft Lewis bases) and low-valent transition metal ions (soft Lewis acids, such as Co^{2+}, Ni^{2+}, Cu^{2+}, and Zn^{2+}) based on hard–soft–acid–base (HSAB) theory.[37]

Meanwhile, catalytically active ligands such as porphyrins can be introduced into MOFs, as well as modulating the pore environment and pore structure to regulate the catalytic performance of monometallic MOFs. In addition, to enhance the electrocatalytic activity of MOFs, the formation of MOFs with bimetallic active sites using binuclear metal clusters/ions is an effective strategy because the synergistic effect between different metal centers can modulate the electronic structure and surface states of metal centers for the purpose of optimizing the catalytic performance. Thanks to their unique pores and abundant functional groups, MOFs are good supports for loading metal nanoparticles or metal monoatoms. Compounding with inorganic active materials with catalytic activity is also an efficient strategy to enhance catalytic activity. In recent years, based on the most prominent weaknesses of MOFs for electrocatalysis applications: stability, conductivity and mass transfer rate, researchers have made breakthroughs through several design strategies, including mono-/bimetallic MOFs, MOFs as supports and MOF-based composite catalysts, which are categorized in this section and the following sections to highlight representative research results.

3.1 Mono/bimetallic MOFs

In order to solve the key problem of insulating MOFs themselves, a common approach to improve the conductivity of MOFs is to design conductive MOFs, which will be mentioned several times in this section and in the following sections for example generalization. Among them, the strategies for designing conductive MOFs generally include: 1. introduction of conductive guest molecules in the pore channels of MOFs, 2. electron energy off-domain in the lattice, 3. charge transfer between planes through interlayer π–π stacking to improve energy matching and orbital overlap between metals and ligands, and 4. Design of constant electron transfer between metals and ligands. The more common method is to design two-dimensional conductive nanosheets, and the synthesis methods are generally top-down (peeling effect is achieved by applying external forces to disrupt the weak interlayer interaction forces) and bottom-up (direct synthesis of two-dimensional MOFs by designing metals and ligands). In 2017, Bu and co-workers reported two new Co MOFs with different coordination and lattice patterns in two- and three-dimensional structures: CTGU-5 and CTGU-6 (Fig. 1a).[38] After physical doping with some acetylene black, AB&CTGU-5 (1 : 4) exhibited optimal HER catalytic performance in 0.5 M H_2SO_4 with an onset potential of 18 mV (Fig. 1b), an overpotential of only 44 mV required to reach 10 mA cm^{-2}, and a low Tafel slope of 45 mV dec^{-1}, making this Co-MOF one of the best 2D MOFs known for its performance.

Both Qiao and Zhang's groups summarized the unique advantages of 2D materials,[39,40] which include the construction of 2D conducting MOFs as an important strategy for electrocatalytic applications. Meanwhile, the addition of a metal to monometallic MOFs can significantly enhance the overall HER catalytic activity. Currently, transition metal-based MOFs are the main research targets of bimetallic MOF electrocatalysts, among which Ni-based and Fe-based MOFs are more prominent. However, in general bimetallic MOF catalysts usually have better HER catalytic activity only in alkaline media, while bimetallic MOFs in acidic media are less reported. In 2021, Chen *et al.* formed a two-dimensional hexagonal lattice by crystallizing Cu-CAT (catecholate) in the triangular space group *P*3*c*1 and Cu ions coordinated to 2,3,6,7,10,11-hexahydroxytriphenylene, creating a two-dimensional structure with excellent electrical conductivity.[41] Then, Co was introduced into Cu-CAT in an alternating structure (Fig. 1c), and CuCo-CAT/CC was obtained by *in situ* growth on carbon cloth. When the electrolyte is 1.0 M KOH, CuCo-CAT/CC requires only 52 mV overpotential to reach 10 mA cm^{-2}, which is superior to monometallic nanorod arrays (Fig. 1d). DFT calculations demonstrate that the introduction of Co greatly enhances the

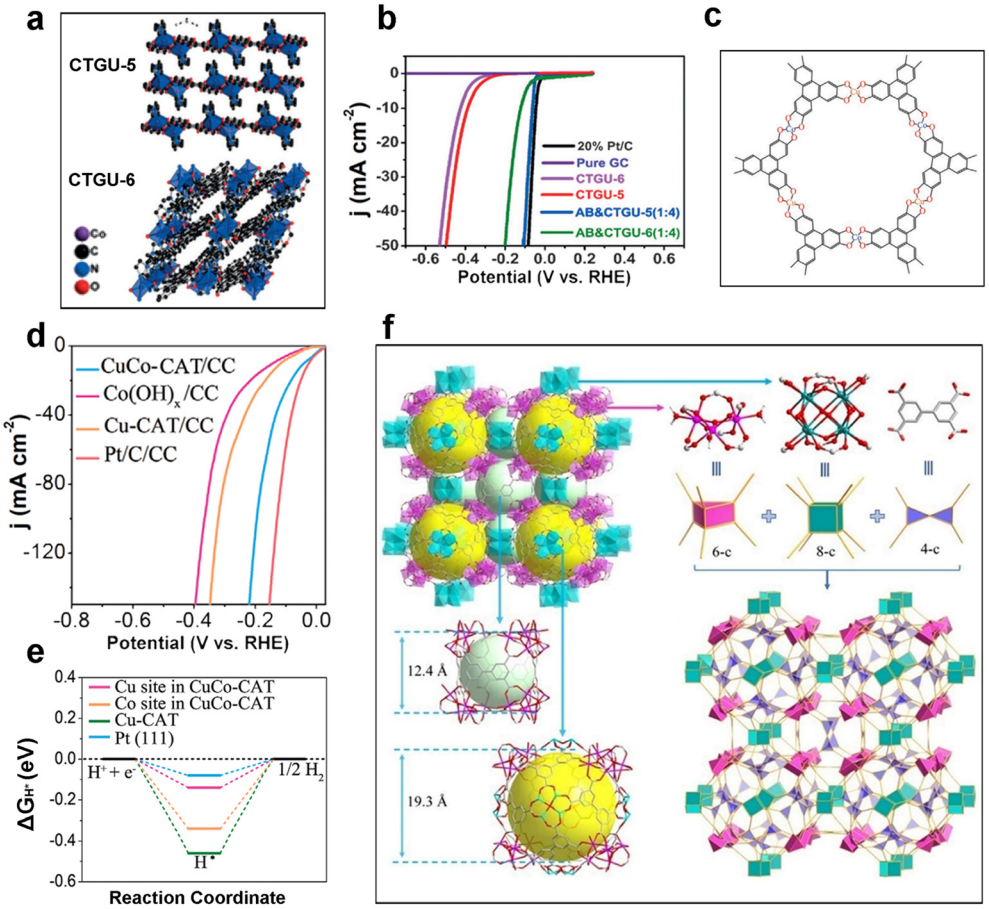

Fig. 1 MOF-based HER electrocatalysts. (a) Crystal structure diagrams of two isomeric Co MOFs (CTGU-5 and CTGU-6); (b) LSV curves of CTGU-5, CTGU-6 and other comparison samples for HER tests in 0.5 M H_2SO_4. Reproduced with permission.[38] Copyright 2017, Wiley-VCH; (c) the structure of CuCo-CAT; (d) LSV curves of CuCo-CAT/CC and other comparison samples for HER tests in 1.0 M KOH; (e) calculated hydrogen adsorption free energy diagram for Cu and Co sites in CuCo-CAT, Cu-CAT and Pt(111). Reproduced with permission.[41] Copyright 2021, Wiley-VCH; (f) crystal structure of Ni-NKU-101. Reproduced with permission.[43] Copyright 2022, Wiley-VCH.

hydrogen adsorption energy (ΔG_{H^*}), which in turn accelerates the Volmer step of the HER (Fig. 1e). Therefore, the design of MOF-based hydrogen evolution reaction electrocatalysts can first calculate the hydrogen adsorption energy, Gibbs free energy of the key steps of the HER and synergistic effects based on DFT, and then guide the synthesis of potential mono- or bimetallic MOF electrocatalysts from the perspective of the reaction mechanism, which will largely facilitate the exploration of excellent catalysts. Also as a transition metal, Fe-MOFs exhibit promising electrocatalytic hydrogen evolution activity. Chen and co-workers investigated the hydrolysis performance of different divalent metals with Fe-based bimetallic MOFs by a one-pot hydrothermal method in 2022.[42] The highest ECSA of the optimal CdFe-MOF was obtained to be 3.02 mF cm^{-2}, with a TOF value of 0.325 s^{-1} at 280 mV, with an overpotential of only 148 mV required to reach 10 mA cm^{-2}. Also based on DFT calculations, it was revealed that the introduction of Cd atoms greatly reduces the hydrogen adsorption energy. This work provides guidance for the design of transition metal-based bimetallic MOFs.

Precise design of tetracarboxylic acid groups of 3,3′,5,5′-biphenyltetracarboxylic acid ligands can enhance the metal center–ligand ratio, thus optimizing the density of metal active sites in MOFs and enabling more efficient utilization of active sites. In 2022, Cheng and co-workers used trinuclear and octanuclear nickel clusters as secondary building blocks, which were interconnected by 4-connected ligands to prepare bimetallic cage-based MOFs (size 12.4 and 19.3 Å, respectively) (Fig. 1f).[43] Thanks to the synergistic catalytic utility between the two metals, Cu_xNi_{1-x}-NKU-101 exhibited HER electrocatalytic performance superior to other M_xNi_{1-x}-NKU-101 catalysts in acidic media. As-prepared $Cu_{0.19}Ni_{0.81}$-NKU-101 reached an overpotential of 324 mV at 10 mA cm^{-2} and a Tafel slope of 131 mV dec^{-1}, while having the smallest charge transfer rate and the largest exchange current density (j_0).

3.2 MOF-based composites

MOF composites with inorganic reactive materials are one of the effective ways to enhance performance and have been

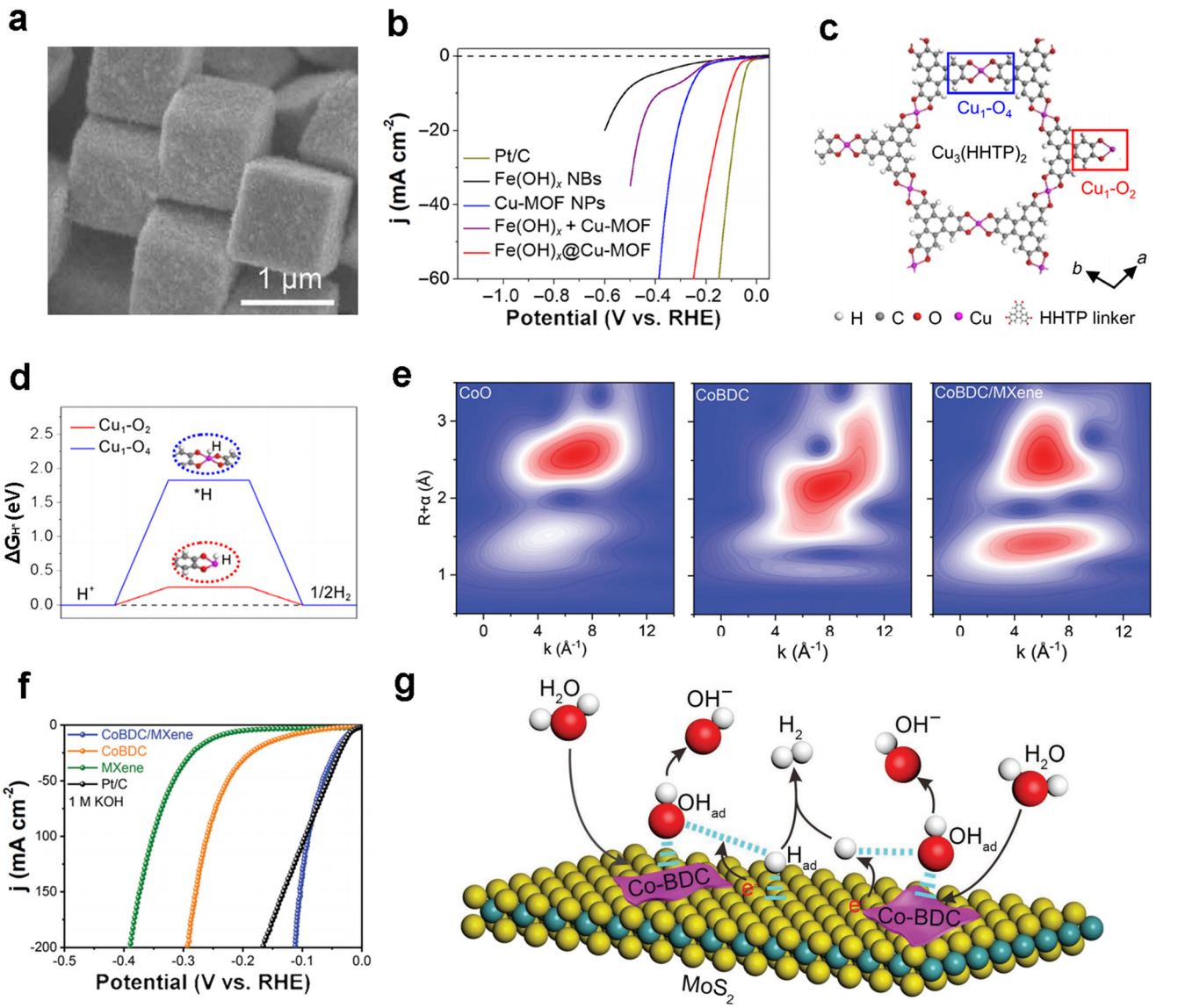

Fig. 2 MOF-based HER electrocatalysts. (a) FESEM images of sample $Fe(OH)_x$@Cu-MOF NBs; (b) LSV curves of Pt/C, $Fe(OH)_x$ NBs, Cu-MOF NPs, $Fe(OH)_x$ + Cu-MOF, and $Fe(OH)_x$@Cu-MOF NBs in 1.0 M KOH; (c) crystal structure of unsaturated Cu-MOF[$Cu_3(HHTP)_2$] observed along the *c*-axis; (d) ΔG of adsorbed *H calculated at the Cu sites of Cu_1–O_4 and Cu_1–O_2 centers. Reproduced with permission.[44] Copyright 2021, American Association for the Advancement of Science; (e) wavelet transform plots of k^3-weighted EXAFS signals for CoO, CoBDC and CoBDC/MXene; (f) LSV curves of Pt/C, MXene, CoBDC and CoBDC/MXene for HER tests in 1.0 M KOH. Reproduced with permission.[45] Copyright 2022, Wiley-VCH; (g) schematic diagram of the basic HER catalytic mechanism of the Co-BDC/MoS_2 composite. Reproduced with permission.[46] Copyright 2019, Wiley-VCH.

extensively investigated. In 2021, Lou *et al.* cleverly designed ultrathin tetragonal composites of a conductive copper-based MOF (Cu-MOF) with high carrier mobility and excellent conductivity loaded on the surface of iron hydroxide [$Fe(OH)_x$] nanoboxes by a simple template-based solvothermal reaction and redox post-processing strategy (Fig. 2a).[44] As-prepared $Fe(OH)_x$@Cu-MOF exhibited satisfactory HER catalytic activity, with an overpotential of 112 mV at a current density of 10 mA cm^{-2} (Fig. 2b), along with a small Tafel slope of 76 mV dec^{-1}. The authors modeled the crystal structure of the unsaturated Cu MOF (Fig. 2c) and found by DFT theoretical calculations combined with synchrotron radiation tests that a highly efficient and optimized HER was achieved due to the highly exposed ligand unsaturated Cu_1–O_2 center that greatly reduced the hydrogen adsorption energy (ΔG_{H^*}) (Fig. 2d).

MXenes show promising applications in electrocatalysis because of their excellent electrical conductivity and the abundance of functional groups (–F, –O, –OH, *etc.*) on their surface. Peng and co-workers constructed novel 2D/2D CoBDC/MXene (BDC stands for 1,4-benzenedicarboxylate, $C_8H_4O_4$) composites using *in situ* growth methods in 2022.[45] The wavelet transform spectroscopy revealed strong interactions at the interface resulting in a change in the electronic structure (Fig. 2e). The overpotentials required to reach 10 mA cm^{-2} current density for the CoBDC/MXene

Table 1 List of some recently reported MOF-based electrocatalysts for different electrocatalytic reactions

HER electrocatalysts	Overpotential (mV) at 10 mA cm^{-2}	Tafel slope (mV dec^{-1})	Electrolyte	Ref.
D-Ni-MOF	101	50.9	1.0 M KOH	53
Fe–Co–Ni MOF	116	56	1.0 M KOH	54
Fe_2Zn-MOF	221	174	0.1 M KOH	55
HUST-200	131	51	Acidic aqueous medium	56
$Mn_{0.52}Fe_{0.71}$Ni-MOF-74	99	103.8	1.0 M KOH	57
$NiRu_{0.13}$-BDC	34	32	1.0 M KOH	52
2DCo-BDC/MoS_2	248	86	1.0 M KOH	46
Ni-MOF@Pt	43	30	0.5 M H_2SO_4	48
Ni-MOF@Pt	102	88	1.0 M KOH	48
$Fe(OH)_x$@Cu-MOF	112	76	1.0 M KOH	44
CoBDC@MXene	29	46	1.0 M KOH	45
NiFe-MOF	134	—	0.1 M KOH	58

OER electrocatalysts	Overpotential (mV) at 10 mA cm^{-2}	Tafel slope (mV dec^{-1})	Electrolyte	Ref.
Fe–Co–Ni MOF	254	51.3	1.0 M KOH	54
NiCo-UMOFNs	180	42	1.0 M KOH	73
MIL-53(Fe)-2OH	215	45.4	1.0 M KOH	70
Ni_2Fe_1 Sq-zbr-MOFs	230	37.7	1.0 M KOH	74
NiFe-MOF/G	258	49	1.0 M KOH	77
Ni-BDC-1R	225	83	1.0 M KOH	81
FN-2 electrocatalyst	275	56.7	1.0 M KOH	82
Co-MOF-NK	324	77.5	1.0 M KOH	72
Co-MOF/NF	270	75	1.0 M KOH	71
FeNi-MOF	239@50 mA cm^{-2}	52.4	1.0 M KOH	75
D-Ni-MOF	219	48.2	1.0 M KOH	53
$Ti_3C_2T_x$–CoBDC hybrid	410	48.2	0.1 M KOH	78
M-PCNB/CC	232	32	1.0 M KOH	80
$CoCl_2$@Th-BPYDC	388	94	0.1 M $HClO_4$	79
$A_{2.7}$B-MOF-$FeCo_{1.6}$	288	39	1.0 M KOH	83

ORR electrocatalysts	$E_{1/2}$ (V *vs.* RHE)	Tafel slope (mV dec^{-1})	Electrolyte	Ref.
$Co_3(HADQ)_2$ MOF	0.825	79	0.5 M H_2SO_4	88
Pt/C	0.835	76	0.5 M H_2SO_4	88
PCN-226	0.75	58.9	0.1 M KOH	89
NiZn MOFs	—	76	0.1 M KOH	90
Ni_1Fe_2-MOF@GC	0.676	—	0.1 M KOH	91
PcCu–O_8–Co/CNT	0.83	61	0.1 M KOH	95
Pt/C	0.85	68	0.1 M KOH	95
MCCF/NiMn-MOFs	0.73	86	0.1 M KOH	94
CoNiMOF/rGO	—	67	0.1 M KOH	96
1@ZIF-8	0.79	53	0.1 M KOH	98
1@ZIF-67	0.79	56.2	0.1 M KOH	98
4.3%-NiFe-MOF	0.83	70	0.1 M KOH	99

NRR electrocatalysts	NH_3 yield rate (μg h^{-1} mg_{cat}^{-1})	FE (%)	Electrolyte	Ref.
MOF(Fe)	2.12×10^{-9} mol s^{-1} cm^{-2}	1.43	2.0 M KOH	114
HKUST-1	46.63	2.45	0.1 M Na_2SO_4	105
Defective UiO-66-NH_2	52.81	85.21	0.1 M Na_2SO_4	115
In-MOF	24.70	6.72	pH = 1	116
In-MOF	64.73	12.23	pH = 7	116
In-MOF	79.2	14.98	pH = 12	116
NiFe-MOF	9.3	11.5	0.1 M $NaHCO_3$	107
HT Au@MOF	49.5	60.9	0.1 M Na_2SO_4	112
OPA-PCN-222(Fe)	49.7	17.2	0.1 M HCl	106
NH_2-MIL-88B-Fe	1.205×10^{-10} mol s^{-1} cm^{-2}	12.45	0.1 M Na_2SO_4	104
ZIF-67@Ti_3C_2	6.52 μmol h^{-1} cm^{-2}	20.2	0.1 M KOH	109
MIL-101(Fe)/MoS_3	25.7	36.71	0.1 M HCl	111
NPG@ZIF-8	28.7	44	0.1 M Na_2SO_4	113
CNT@UIO-66	3.811	15.14	0.05 M H_2SO_4	110
NCNT@UIO-66	6.081	18.13	0.05 M H_2SO_4	110
NCNT@MIL-101(Fe)	5.514	25.15	0.05 M H_2SO_4	110
CNT@MIL-101(Fe)	6.97	37.28	0.05 M H_2SO_4	110
Co_3Fe-MOF	8.79	25.64	0.1 M KOH	108

composite in 1.0 M KOH are 29 mV (Fig. 2f), respectively, achieving HER performance close to Pt/C, which is of great significance for the development of MOF-based electrocatalysts for the hydrogen evolution reaction (Table 1). Moreover, Qiao *et al.* also employed a Co-BDC MOF with the two-dimensional material MoS_2 to make a Co-BDC/MoS_2 composite,[46] where Co-BDC acts as an electron donor and enables partial phase transfer from 2H-MoS_2 to 1T-MoS_2 by coupling Co-BDC with MoS_2, which activates the otherwise inert substrate while enhancing the electrical conductivity and thus accelerating the basic hydrolysis step of the decisive step in the HER (Fig. 2g). Therefore, compositing MOFs with inorganic functional catalytic materials is currently a promising strategy for designing HER electrocatalysts, which is not only limited to the HER but also can be extended to other electrocatalytic fields.

3.3 MOFs as supports

The pore size of MOFs can be tuned to support nanoparticles/single atoms to optimize the electron transfer in electrocatalysis, while the active MOF can interact with the nanoparticles/single atoms to further improve the catalytic activity/selectivity. In 2021, Peng and co-workers cleverly anchored a series of metal nanoparticles (NPs) on a nickel-based MOF (Fig. 3a).[47] The optimal Ru@Ni-MOF only needs 22 mV to reach 10 mA cm^{-2} in 1.0 M KOH and has a Tafel slope (40 mV dec^{-1}) smaller than Pt/C (42 mV dec^{-1}). Furthermore, the Ru@Ni-MOF also has good HER stability at different pH values, running at a constant 100 mA cm^{-2} for 24 h with almost no decay. The outstanding activity and stability of the Ru@Ni-MOF are rare for MOF-based electrocatalytic HER catalysts. The authors jointly confirmed

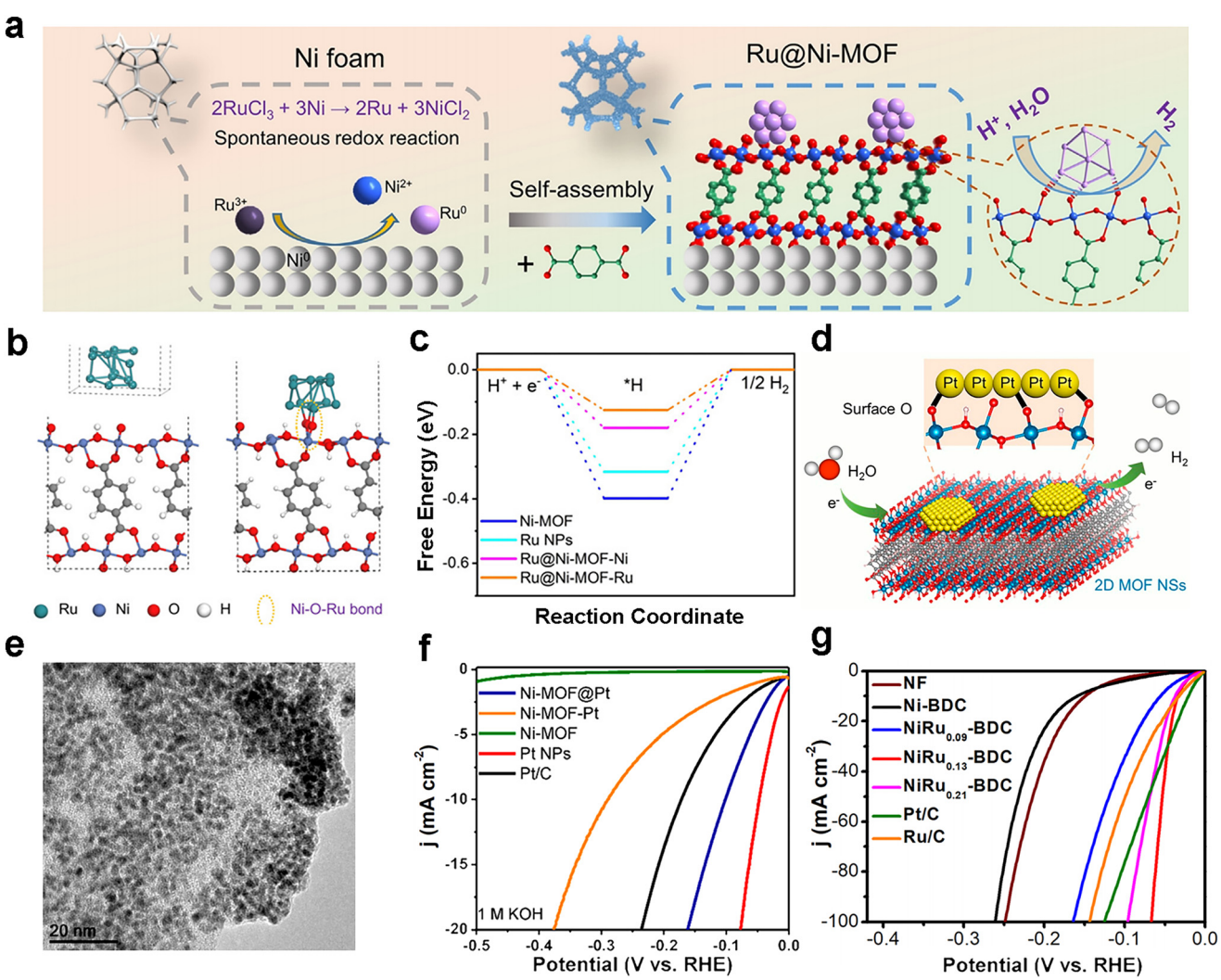

Fig. 3 MOF-based HER electrocatalysts. (a) Schematic diagram of the synthesis of Ru@Ni-MOF nanosheets; (b) the constructed structural models of Ru NPs, Ni-MOF and Ru@Ni-MOF; (c) calculated hydrogen adsorption free energy diagram for Ni-MOF, Ru NPs, Ru@Ni-MOF-Ni, and Ru@Ni-MOF-Ru. Reproduced with permission.[47] Copyright 2021, Wiley-VCH; (d) schematic diagram of the HER process of Ni-MOF@Pt; (e) TEM image of Ni-MOF@Pt; (f) LSV curves of Ni-MOF@Pt and other comparison samples for HER tests in 1.0 M KOH. Reproduced with permission.[48] Copyright 2019, American Chemical Society; (g) LSV curves of $NiRu_{0.13}$-BDC and other comparison samples for HER tests in 1.0 M PBS. Reproduced with permission.[52] Copyright 2021, Springer Nature.

the bonding mode of Ni–O–Ru bonds and the interaction forces between the Ru NPs and Ni-MOF that modulate the electronic structure of Ru and Ni atoms by XPS, EXAFS and FT-IR characterization. Then, a model was developed for the theoretical calculation of the hydrogen adsorption free energy (Fig. 3b and c), revealing that the optimized electronic structure of Ni–O–Ru bonding achieves the optimization of the free energy of water and hydrogen evolution reaction. Another study optimized the coordination environment and electronic structure of noble metal nanoparticles by designing two-dimensional conducting MOFs as supports (Fig. 3d).[48] The authors used a surfactant-free method to grow Pt nanoparticles (nanoparticle size around 3 nm, Fig. 3e) on two-dimensional MOF nanosheets. The synthesized Ni-MOF@Pt exhibits excellent HER performance, requiring an overpotential of 43 mV and a Tafel slope of only 30 mV dec^{-1} to reach 10 mA cm^{-2} in acidic media, and an overpotential of 102 mV and a Tafel slope of 88 mV dec^{-1} to reach 10 mA cm^{-2} in alkaline media (Fig. 3f). This work shows great promise for supporting metal nanoparticles with two-dimensional conductive MOFs.

Recently, single-atom catalysts (SACs) have attracted much attention in the construction of electrocatalysts because they can maximize the utilization of atomic active sites, thus modifying the interaction between the monometallic atoms and the carrier and thus providing excellent catalytic activity to the material.[49,50] In addition, uniform loading of single atoms can be achieved on the basis of the original material without losing the original morphological and structural features, which implies that loading single atoms on MOFs is a feasible strategy.[51] In 2021, Su and co-workers loaded atomically dispersed Ru into a Ni-BDC MOF, and obtained a $NiRu_{0.13}$-BDC electrocatalyst,[52] which showed outstanding performance. When the electrolyte is 1 M phosphate buffer saline (PBS) solution, it has a low overpotential of 36 mV at a current density of 10 mA cm^{-2} and an outstanding Tafel slope of 32 mV dec^{-1} (Fig. 3g). Furthermore, it was demonstrated by DFT calculations that the strategy of loading atomically dispersed Ru onto the MOF promoted the adsorption of H_2O and enhanced the water dissociation energy, while it optimized the hydrogen adsorption energy, and ΔG_{H^*} approached the thermal neutrality 0, thus effectively enhancing the electrocatalytic HER performance. This strategy of *in situ* supporting single atoms on top of MOF supports to design efficient MOF electrocatalysts provides a new avenue for researchers.

Hence, the nanostructures of MOFs can be rationally controlled and prepared because their structure, pore environment and morphology are tunable, which greatly affects the electrocatalytic hydrogen evolution performance. Furthermore, strategies such as compositing the prepared MOFs with conductive inorganic materials or supporting metal nanoparticles or single atoms with MOFs as supports may mechanistically enhance the hydrogen adsorption energy, optimize the water dissociation energy and thus promote the overall hydrogen evolution activity. Therefore, pure MOF-based materials are considered as promising candidates for electrocatalytic hydrogen precipitation. However, several issues need to be noted: 1. it is still necessary to modulate metals and ligands to expand the variety of MOF materials and further modulate the morphology through different strategies to obtain more optimized MOF materials. 2. Overall, despite the great efforts in hydrogen evolution under strongly acidic and alkaline conditions, the performance of the electrocatalytic HER is still far from the industrial and large-scale hydrogen production level, and further attention can be paid to the design of more stable MOFs to withstand long time voltage operation as well as electrolyte erosion.

4 MOF-based electrocatalysts for the hydrogen oxidation reaction

The hydrogen oxidation reaction (HOR) is one of the key processes in anion-exchange membrane fuel cells. To date, platinum-based materials remain the most efficient and stable benchmark catalysts.[59] As the reverse reaction of the HER, the HOR has a similar reaction type and mechanism to the HER. The HOR is a two-electron transfer reaction with a reaction intermediate containing multiple hydrogen types, depending on the pH of the electrolyte. The reaction processes of the HOR at different pH values are summarized as follows:

Acidic:

$$H_2 \rightarrow 2H^+ + 2e^-$$

In acidic media, it generally consists of two of the following three steps (Tafel/Volmer or Heyrovsky/Volmer).

$$\text{Tafel step: } H_2 \rightarrow 2H^*$$

$$\text{Heyrovsky: } H_2 \rightarrow H^* + e^- + H^+$$

$$\text{Volmer step: } H^* \rightarrow e^- + H^+$$

Alkaline:

$$H_2 + 2OH^- \rightarrow 2H_2O + 2e^-$$

In alkaline media, the Heyrovsky and Volmer steps are often described with hydroxides as reactants:

$$\text{Tafel step: } H_2 \rightarrow 2H^*$$

$$\text{Heyrovsky: } H_2 + OH^- \rightarrow H^* + e^- + H_2O$$

$$\text{Volmer step: } H^* + OH^- \rightarrow e^- + H_2O$$

Specifically, the three basic steps are involved in the overall HOR process: first, the formation of the H* intermediate *via* the Tafel or Heyrovsky step, followed by the formation of water in the Volmer step. Since H* formation is required in the Tafel and Heyrovsky steps, an excellent HOR electrocatalyst needs to have the right value for hydrogen chemisorption. If the proton adsorption energy is too strong at this point, it is not favorable for the later Volmer process, and if it is too weak, the proton detaches before the reaction occurs. Therefore, hydrogen binding energy (HBE) is generally considered as a key descriptor for assessing HOR kinetics. In addition, alkaline conditions involve hydroxide adsorption, so the HOR under alkaline conditions must consider the adsorption energy of hydroxide. Therefore, the mainstream considers the HOR with a bifunctional catalytic theory, *i.e.*, the design of electrocatalysts that simultaneously balance the hydrogen adsorption energy as well as the hydroxyl adsorption energy.[60]

Since the electrocatalytic hydrogen oxidation reaction is in the nascent stage of development, up to now, almost all of the reported MOF-based HOR electrocatalysts are MOF derivatives, *i.e.*, MOFs are converted to carbon-based materials/monoatomic doped materials, *etc.* by high-temperature calcination, such as Ni@Oi–Ni,[61] Ni/NiO/C,[62] Ni–H_2–NH_3,[59] *etc.* However, the process of obtaining derivatives by pyrolysis of MOFs is complicated and the destruction of the coordination environment inside MOFs at high temperatures makes the structure difficult to control precisely. MOFs have the advantages of regular periodic arrangement structure and precisely controllable pore structures, as well as ligand functionalization and high specific surface area, which can enable rapid hydrogen transport within the pores, promote gas diffusion, and improve catalytic activity. Therefore, MOFs will play a key role in the future development of the anode oxidation reaction of anion-exchange membrane fuel cells, *i.e.*, the hydrogen oxidation reaction.

5 MOF-based electrocatalysts for the oxygen evolution reaction

The oxygen evolution reaction (OER) is an anodic reaction for electrocatalytic water splitting.[63,64] The OER process involves four-electron transfer and is a kinetic hysteresis process, which is more complex than the hydrogen evolution reaction. The OER requires a larger overpotential to complete the reaction in practice. The following is a summary of the four-electron reaction process of oxygen evolution from electrolytic water.

Acidic:

$$\text{Total reaction: } 2H_2O \rightarrow O_2 + 4e^- + 2H^+$$

$$\text{Reaction process: } * + H_2O \rightarrow OH^* + e^- + H^+$$

$$OH^* \rightarrow O^* + H^+ + e^-$$

$$O^* + H_2O \rightarrow OOH^* + e^- + H^+$$

$$OOH^* \rightarrow 2O^* + e^- + H^+$$

$$OOH^* + OH^- \rightarrow H_2O + O_2 + e^-$$

$$O_2^* \rightarrow * + O_2$$

Alkaline:

$$\text{Total reaction: } 4OH^- \rightarrow O_2 + 4e^- + 2H_2O$$

$$\text{Reaction process: } * + OH^- \rightarrow OH^* + e^-$$

$$OH^* + OH^- \rightarrow H_2O + O^* + e^-$$

$$O_2^* \rightarrow * + O_2$$

Since the first step of the reaction in acidic media involves the decomposition of water molecules resulting in slow reaction kinetics, while that in alkaline media does not involve the decomposition of water molecules, the oxygen evolution reaction is more likely to occur in acidic media than in alkaline media. For the reaction mechanism of the OER, taking the hydrogen evolution reaction in an alkaline medium as an example: the OER generally starts with the adsorption of OH^- at the metal site (M) on the catalyst surface and the discharge of OH^- in the adsorbed state, which then reacts with OH^- in solution to form water and adsorbed O* and release an electron. The OH^- anion then reacts with the adsorbed O* to form adsorbed OOH. In addition, as the OH– anion reacts further, adsorbed O_2 and H_2O are formed, and adsorbed O_2 precipitates in the final step.

For MOF-based catalysts, there are several strategies generally developed to enhance the kinetics of hysteretic OERs. One is to construct array nanostructures or prepare a pure MOF into two-dimensional conducting nanosheets, the second is to construct MOFs with ligand unsaturated metal sites, the third is to modulate different functionalized ligands and to construct multi-metal component MOFs by changing the number of metal ions/metal clusters, and the fourth is to modulate the electronic structure by compounding nanoparticles or inorganic active materials and modulating the interfacial coupling to enable modification/reconfiguration to occur, *etc.*[65,66]

5.1 Monometallic MOFs

The designed reconstruction of the original structure of MOFs to obtain the target structure is a promising strategy to enhance the catalytic performance. This strategy involves the use of *in situ* characterization to monitor the products during the reaction in real time, the morphological changes of MOFs undergoing dynamic reconstruction during electrocatalysis, and the identification of the actual active site of the reaction. The transformation of cobalt sites under the operating conditions of the oxygen evolution reaction was investigated in depth by Lee and co-workers using *in situ* UV-vis and Raman spectroscopy.[67] The tetra-ligand skeleton of ZIF-67 is gradually deconstructed with increasing applied voltage: the tetra-ligand framework is gradually replaced by electrolyte OH^- ions, which are transformed into tetra-ligand α-$Co(OH)_2$ and octa-ligand β-$Co(OH)_2$, and then further oxidized to the high-valent state CoOOH which is the real OER active center and not the original metal node in the MOF. Moreover, *in situ* FT-IR and *in situ* X-ray absorption spectroscopy have been used to monitor the products of the reaction process in real time. For example, Tang *et al.* used *in situ* X-ray absorption spectroscopy (XAS) to investigate the structural transformation of the electrocatalyst $Ni_{0.5}Co_{0.5}$-MOF-74

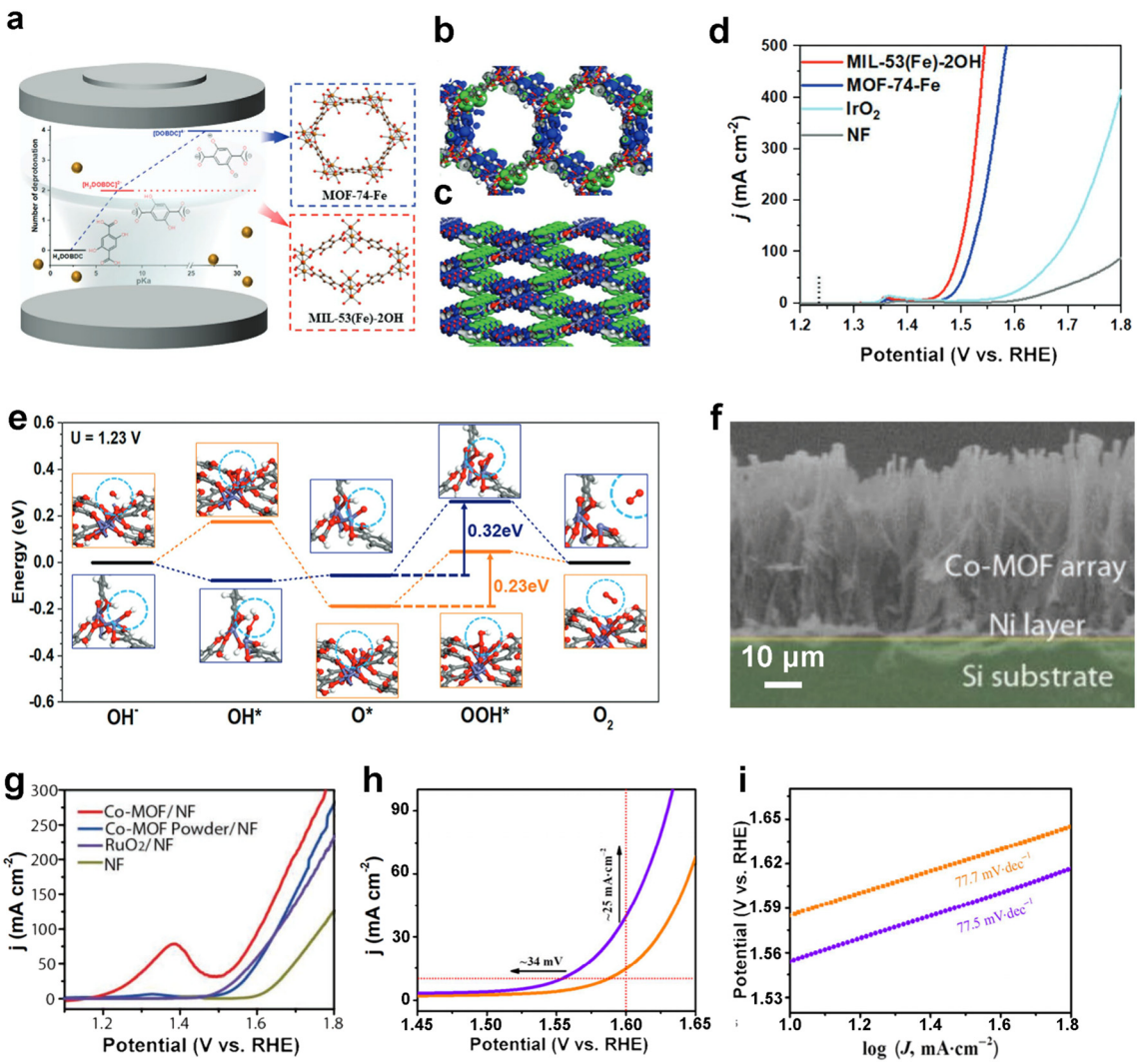

Fig. 4 MOF-based OER electrocatalysts. (a) Schematic diagram of MIL-53(Fe)-2OH and MOF-74-Fe catalysts fabricated. Three-dimensional contour plots of the electron distribution near the Fermi level for (b) MOF-74-Fe and (c) MIL-53(Fe)-2OH. The blue, gray, red, and white spheres represent iron, carbon, oxygen, and hydrogen elements, respectively. The bonding and anti-bonding orbitals are indicated by the blue and green equivalent surfaces, respectively; (d) LSV curves of MIL-53(Fe)-2OH, MOF-74-Fe, IrO_2 and nickel foam (NF) for OER tests in 1.0 M KOH; (e) OER transition states and corresponding free energy calculations for MOF-74-Fe (blue line) and MIL-53(Fe)-2OH (orange line) at U = 1.23 V (blue and orange squares represent the structural changes that occur for MOF-74-Fe and MIL-53(Fe)-2OH, respectively). Reproduced with permission.[70] Copyright 2022, Wiley-VCH; (f) SEM images of Co-MOF nanoarrays; (g) LSV curves of Co-MOF/NF and other samples for OER tests in 1.0 M KOH. Reproduced with permission.[71] Copyright 2019, Wiley-VCH; (h) LSV curves and (i) Tafel plots of Co-MOF-NK (purple) and Co-MOF-K (orange) for OER tests in 1.0 M KOH. Reproduced with permission.[72] Copyright 2021, Springer Nature.

during the OER process.[68] Yuan *et al.* used *in situ* FT-IR spectroscopy to probe the NRR process of N,B-PC following the associative mechanism.[69]

Recently, Yang's group chose to reconfigure the original structure of MOFs to achieve control over monometallic Fe-MOFs,[70] achieving excellent OER activity and stability. Specifically, a precise conversion from phenolic hydroxyl-ligated MOF-74-Fe with hexagonal channels to unliganded MIL-53(Fe)-2OH with rhombic channels was achieved using an *in situ* solvothermal method (Fig. 4a–c). The prepared MIL-53(Fe)-2OH required an overpotential of only 215 mV to reach 10 mA cm^{-2} in 1.0 M KOH (Fig. 4d), while possessing a low Tafel slope of 45.4 mV dec^{-1}. The TOF value at an overpotential of 300 mV is 1.44 s^{-1}. Theoretical simulations of the OER transition state reveal that the rate-determining step (RDS) of MIL-53(Fe)-2OH is the O* to OOH* transition step, which achieves energy optimization after structural reconstruction (Fig. 4e).

Previously, our group chose Co^{2+} and the ligand thiophene dicarboxylic acid (H_2TDC) to construct an ultra-long array of highly oriented (maximum length of 46 μm) quasi-two-dimensional Co-MOF nanoarrays (Fig. 4f).[71] It was found that Co-MOF/NF (NF stands for nickel foam) grown on top of nickel foam required 270 and 317 mV overpotentials to reach 10 and 50 mA cm^{-2}, respectively, which is superior to commercial RuO_2 (Fig. 4g). This work created a nanoarray OER catalyst with greatly improved ion and electron transport quality, confirming the versatility and universality of strategies for MOF nanoarray growth. In another study, our group investigated the enhancement of OER catalytic activity

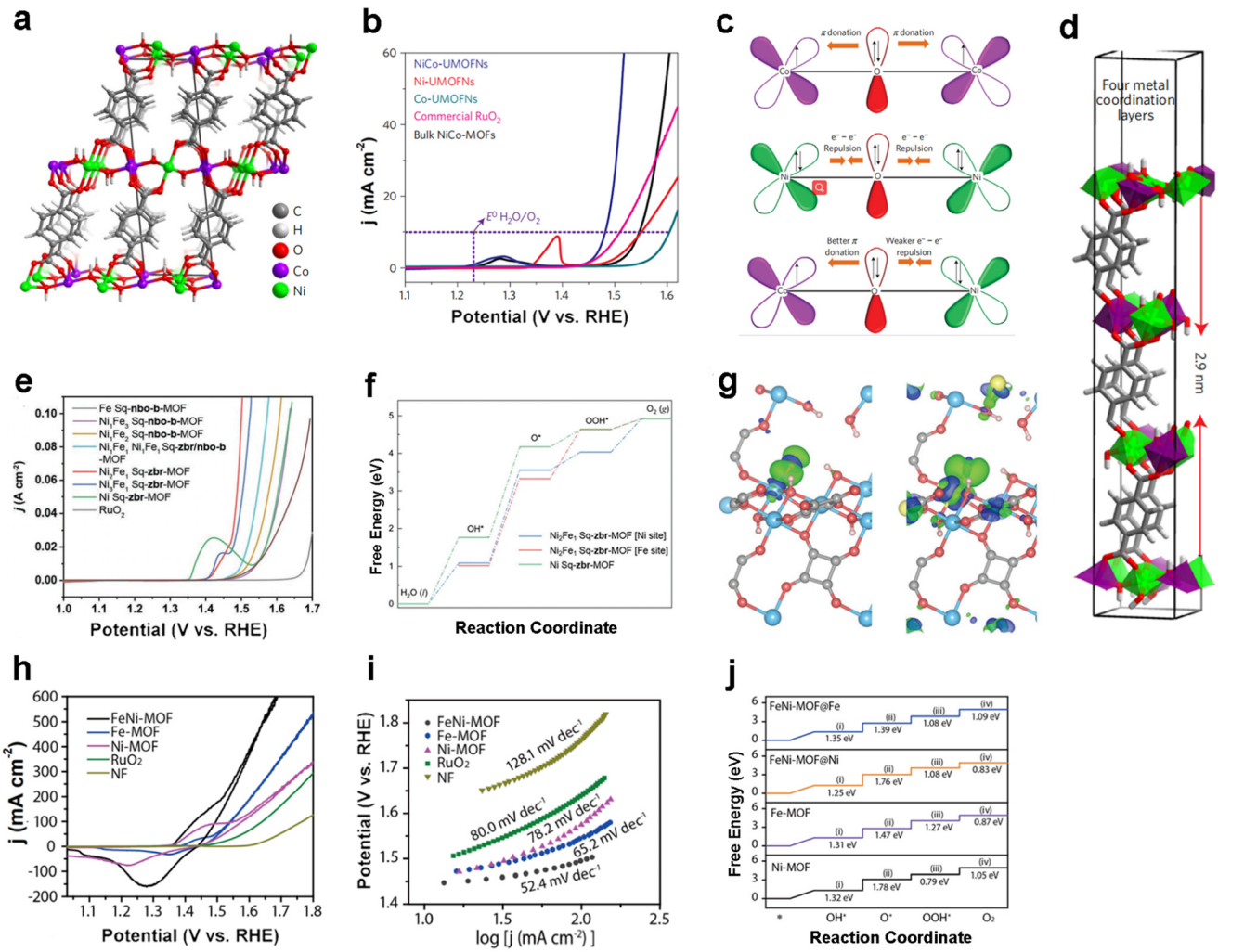

Fig. 5 MOF-based OER electrocatalysts. (a) Crystal structure of NiCo-UMOFNs; (b) LSV curves of NiCo-UMOFNs and other samples for OER tests in 1.0 M KOH; (c) schematic diagram of the electronic coupling between Co and Ni in UMOFNs; (d) theoretical thickness of NiCo-UMOFNs with four metal coordination layers. Reproduced with permission.[73] Copyright 2016, Springer Nature; (e) LSV curves of Fe–Ni Sq-MOFs and other samples for OER tests in 1.0 M KOH; (f) calculated OER standard free energy diagrams for Ni-, Ni_2Fe–Ni-site and Ni_2Fe–Fe-site Sq-MOFs at U = 0 V; (g) difference of charge density of O* on Ni- (left) and Ni_2Fe–Fe-site (right) Sq-zbr-MOFs with the isosurface = 0.005 e $Å^{-2}$ (green and blue shadows show electron accumulation and electron depletion, respectively). Reproduced with permission.[74] Copyright 2022, Wiley-VCH; (h) CV curves and (i) Tafel plot of FeNi-MOF nanoarrays and other samples for OER tests in 1.0 M KOH; (j) calculated OER free energy diagrams for the surfaces of FeNi-MOFs, Fez-MOFs and Ni-MOFs. Reproduced with permission.[75] Copyright 2021, American Chemical Society.

of MOFs induced by the steric hindrance effect of Nafion. Co-MOF-NK obtained by mixing a Co-MOF with Nafion in an alkaline hydrolysis process (AHP) exhibited superior OER performance to Co-MOF-K prepared by immersing Co-MOF nanoribbons in 1.0 M KOH (Fig. 4h and i).[72]

5.2 Bimetallic MOFs

Tang's group enhanced the electrocatalytic OER properties by constructing coordinated unsaturated sites as well as by constructing two-dimensional conducting MOF nanosheets with Ni and Co sites as the active centers of the OER.[73] In detail, the authors used a simple sonication approach to cast nickel–cobalt bimetallic organic frameworks with an ultrathin nanosheet morphology (NiCo-UMOFNs), whose real thickness is about 3.1 nm close to the theoretical thickness of 2.9 nm (Fig. 5d). From the crystal structure of NiCo-MOFs (Fig. 5a), both Co and Ni atoms are octahedra coordinated by six O atoms, and the ultrathin NiCo-MOFs will likely produce coordination unsaturated metal sites on the exposed surface due to the partially terminated BDC coordination bonding with the surface metal atoms. When the electrolyte is 1.0 M KOH, NiCo-MOFs require an overpotential of only 180 mV to reach a current density of 10 mA cm^{-2} (Fig. 5b), which is superior to the commercialized RuO_2 catalysts. After the formation of bimetallic-UMOFNs, the occupancy of the eg-orbitals of the coordination unsaturated metal is optimized, while the strong coupling effect between Co and Ni contributes to the performance of the OER (Fig. 5c).

Besides the construction of two-dimensional conducting MOFs as well as three-dimensional conventional MOFs, one-dimensional MOFs have also received a great deal of attention. In 2022, Eddaoudi and co-workers constructed bimetallic Sq-zbr-MOFs with a zbr topology, which possesses a one-dimensional chain-like morphology with more charge transport capability and adequate active site exposure than conventional three-dimensional MOFs.[74] For the OER, Ni_2Fe_1 Sq-zbr-MOFs require a low overpotential of 230 mV to reach 10 mA cm^{-2} (Fig. 5e), while having a very low Tafel slope of 37.7 mV dec^{-1}, achieving OER performance beyond that of commercial RuO_2 catalysts. It also has good stability. The calculated Gibbs free energy of the transition state of the four-electron OER demonstrates that H* → O* is the rate-determining step (RDS) for all Sq-zbr-MOFs and that the Ni_2-Fe_1–Fe-site Sq-zbr MOF overcomes this step exhibiting the lowest energy with Fe as the main catalytically active site for the OER (Fig. 5f). The difference in charge density induced by O adsorbed at the active site in Fig. 5g reveals the transfer of electrons from the metal active site to O*, thus optimizing the adsorption energy of the intermediate, which in turn facilitates the OER process.

Moreover, our group designed bimetallic FeNi-MOF nanoarrays, which are structurally stable and have excellent OER catalyst performance.[75] The as-prepared FeNi-MOF requires low overpotentials of 239 and 308 mV to reach 50 and 200 mA cm^{-2} current densities, respectively (Fig. 5h). Meanwhile, the FeNi-MOF has a Tafel slope of 52.4 mV dec^{-1} (Fig. 5i), which is lower than that of most of the reported electrocatalysts (Table 1). Surprisingly, the FeNi-MOF was stable for 1033 h (>43 days) at 100 mA cm^{-2} and 200 h at 500 mA cm^{-2}, which is brilliant among MOF-based OER electrocatalysts. The OER-rate determining step (RDS) of the Fe-MOF was found by calculating each step of the OER transition state for the formation of *OH to *O intermediates (Fig. 5j) as well as iron as the major active site. The conversion of Fe^{2+} to Fe^{3+} enhanced the oxygen oxidation and accelerated the reaction kinetics, thus improving the catalytic activity of the OER.

5.3 MOF-based composites

Graphene oxide (GO) based materials are considered as one of the excellent composites due to their advantages such as high specific surface area and high electrical conductivity. In 2013, Loh *et al.* constructed Cu-MOF composites doped with GO, and GO provided a good electron transfer medium to make the synthesized composites HER, ORR, and OER trifunctional catalysts, which provided novel paradigm for other researchers.[76] Recently, Zhao and co-workers designed the MOF–graphene nanocomposite NiFe-MOF/G.[77] The ultrafine MOF particles are uniformly dispersed on graphene (Fig. 6a), which is extremely beneficial for the electrocatalytic reaction. Not surprisingly, NiFe-MOF/G showed superiority over the NiFe-MOF alone as well as commercial Ir/C catalysts (Fig. 6b). Theoretical calculations of the transition state of the OER process revealed Fe as the reactive site (Fig. 6c). Huang's group utilized the strategy of constructing two-dimensional conducting MOF nanosheets to enhance the electrical conductivity, while compounding the nanosheets with ultrathin MXene nanosheets to achieve 2D/2D material composites (Fig. 6d).[78] For the OER, the obtained $Ti_3C_2T_x$–CoBDC hybrid possesses a low Tafel slope of 48.2 mV dec^{-1} and a smaller charge transfer resistance, which in turn optimizes the OER performance and achieves the desired goal of surpassing IrO_2 (Fig. 6e).

5.4 MOFs as supports

Compared with Zr(IV) and Hf(IV), Th(IV) exhibits less hydrolysis, so the choice of Th as the metal node for MOF preparation may possess better crystallinity as well as stability. On this basis, in 2022, Luo and co-workers prepared a series of Th-MOF supported semimetallic site catalysts (MCl_2@Th-BPYDC, M = Cu, Co, Ni) by post-metallizing the carrier Th-based MOF (Th-BPYDC) (Fig. 7a and b), which is linked by a Th_6 cluster and a BPYDC ligand.[79] The prepared catalysts all have a well-defined single-crystal structure (Fig. 7c), and the metal sites are near-square planar MN_2Cl_2 coordination geometries that may become double-channel open metal sites, while two rotatable charge-balanced Cl– anions confer a semi-rigid character (Fig. 7d). In 0.1 M $HClO_4$, $CoCl_2$@Th-BPYDC exhibits the optimal OER performance, reaching 10 mA cm^{-2} requiring an

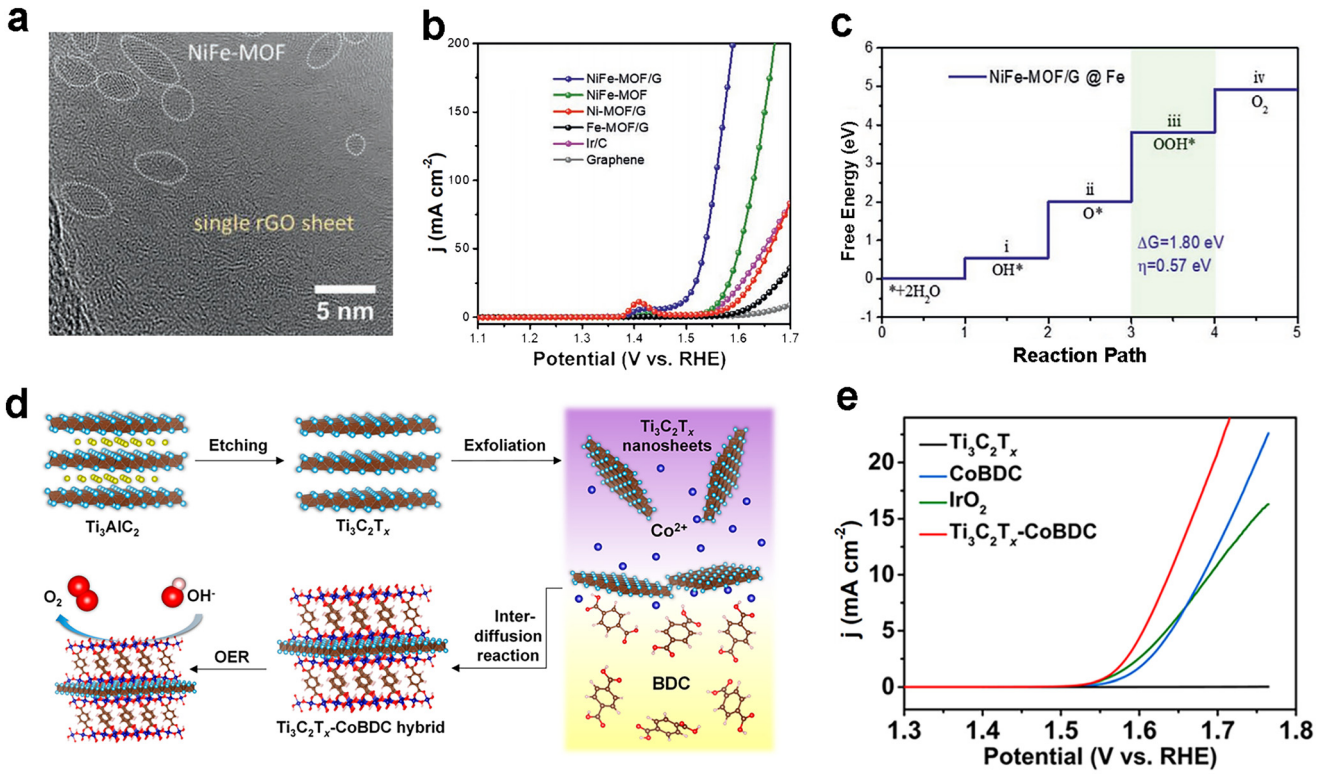

Fig. 6 MOF-based OER electrocatalysts. (a) HRTEM image of NiFe-MOF/G. (b) LSV curves of NiFe-MOF/G and other samples for OER tests in 1.0 M KOH. (c) Calculated free energy diagram for the reaction transition state of the OER process on the Fe site of NiFe-MOF/G. Reproduced with permission.[77] Copyright 2021, Wiley-VCH; (d) schematic diagram of the preparation of $Ti_3C_2T_x$–CoBDC composites for the oxygen evolution reaction. (e) LSV curves of $Ti_3C_2T_x$–CoBDC composites and other samples for OER tests in 0.1 M KOH. Reproduced with permission.[78] Copyright 2017, American Chemical Society.

overpotential of 388 mV (Fig. 7e). In addition, the supporting effect of the Th-BPYDC MOF carrier confers excellent stability to $CoCl_2$@Th-BPYDC. The DFT theoretical calculations deeply probe and corroborate the experimental impression (Fig. 7f). Zhou *et al.* have optimized the electrocatalytic OER performance by cleverly fabricating interfacial Co metal sites using ultrafine $CoFeO_x$ nanoparticles embedded in a monolayer of CoN_4-based MOF lattice.[80] The obtained M-PCNB/CC exhibited superior performance to commercial RuO_2 (Fig. 7g), requiring an overpotential of only 232 mV to reach 10 mA cm^{-2}, while having a very small Tafel slope value of 32 mV dec^{-1} (Fig. 7h), which exceeds most MOF-based OER electrocatalysts, which is significant. Moreover, theoretical calculations further confirm the high activity of the interfacial Co site for the OER (Fig. 7i).

Currently, the strategy of designing suitable MOFs leading to structural reconstruction has shown great potential in electrocatalytic oxygen evolution reactions, because it can regulate the electronic structure of MOFs to facilitate the charge transfer and OER process. In addition, the construction of conductive two-dimensional nanosheets and the design of nanoarray morphologies can accelerate charge transfer and maximize the utilization of active sites. Although remarkable progress has been made in MOF-based catalysts for the OER, the intrinsic mechanism as well as the monitoring of real response and the identification of real active sites needs to be further reported.

6 MOF-based electrocatalysts for the oxygen reduction reaction

The electrocatalytic oxygen reduction reaction is an important cathodic reaction in fuel cells and metal–air cells.[84] However, the slow kinetics of the ORR limits the development of related technology applications. Therefore, the development of high-performance ORR catalysts to break through the key problems of related cells has become one of the core objectives of research.[85] Since the oxygen reduction reaction involves multi-step electron transfer and a variety of oxygen-containing intermediates, it is a complex series of electrochemical processes that have been studied for decades, but the real reaction mechanism has not yet been determined. In general, during the ORR, O_2 is first adsorbed onto the electrode surface, and the adsorbed O_2 gets electrons and is reduced to H_2O or OH^- by a four-electron process; or it is first reduced to hydrogen peroxide (or HO_2^- intermediate) by a 2-electron process, and then reduced to H_2O or OH^- by a 2-electron process.[86]

Four-electron reaction process:

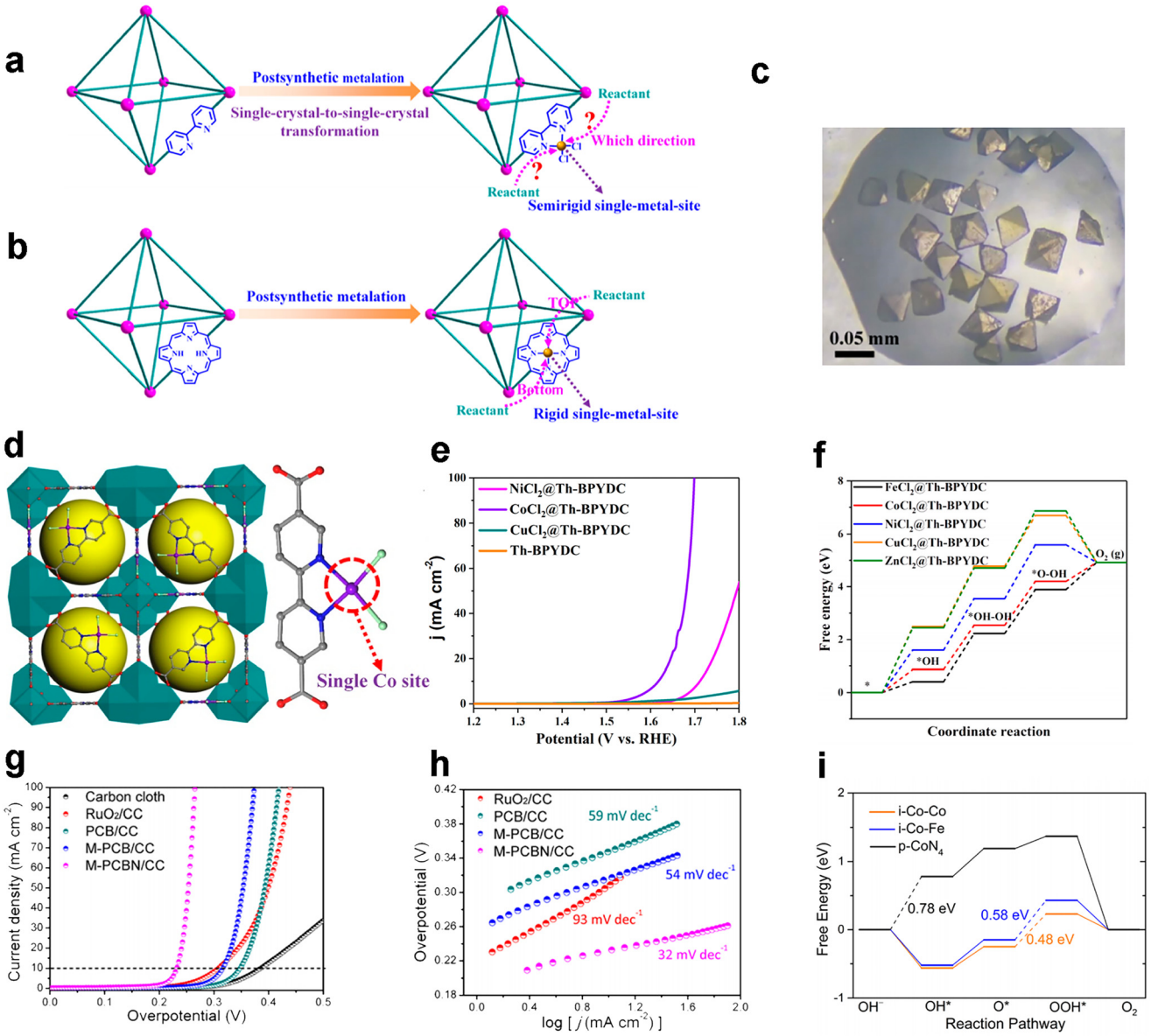

Fig. 7 MOF-based OER electrocatalysts. Routes of reactants accessible to the single-metal site in bipyridyl- (a) and porphyrin-MOFs (b); (c) optical microscopy image of $CoCl_2$@Th-BPYDC; (d) crystal structure of $CoCl_2$@Th-BPYDC; (e) LSV curves of $CoCl_2$@Th-BPYDC and other samples for OER tests in 0.1 M $HClO_4$; (f) calculated free energy diagram for the reaction transition state of the OER process for $CoCl_2$@Th-BPYDC and other samples. Reproduced with permission.[79] Copyright 2022, American Chemical Society; (g) LSV curves and (h) Tafel plot of M-PCBN/CC and other samples for OER tests in 1.0 M KOH; (i) calculated free energy per step diagrams of the OER for i-Co–Co, i-Co–Fe and p-CoN_4 at 1.23 V. Reproduced with permission.[80] Copyright 2020, American Chemical Society.

Acidic: $O_2 + 4H^+ + 4e^- \rightarrow 2H_2O$

Alkaline: $O_2 + 2H_2O + 4e^- \rightarrow 4OH^-$

Two-electron reaction process:

Acidic: $O_2 + 2H^+ + 2e^- \rightarrow H_2O_2$

$H_2O_2 + 2H^+ + 2e^- \rightarrow 2H_2O$

Alkaline: $O_2 + H_2O + 2e^- \rightarrow HO_2^- + OH^-$

$HO_2^- + H_2O + 2e^- \rightarrow 3OH^-$

Since the intermediate HO_2^- produced in the 2-electron process increases the overpotential of the ORR because the reaction needs to provide extra high energy to break the O═O bond, and the H_2O_2 produced in the 2-electron process corrodes the reaction equipment and leads to reduced metal utilization in the metal–air cell, electrocatalysts with high

selectivity should be designed to realize the 4-electron direct reduction reaction process as much as possible.

Platinum-based catalysts are currently the most active benchmark catalysts in ORR electrocatalysis. Nevertheless, the scarcity and high cost of the precious metal platinum on earth limit its large-scale application. Hence, the development of cheap and efficient ORR electrocatalysts is crucial. MOFs are considered as promising ORR electrocatalysts because of their high specific surface area as well as porosity, which can effectively improve oxygen transfer quality as well as provide fast charge transfer channels. In this section, we summarize recent advances in the ORR by classifying monometallic MOFs, bimetallic MOFs, MOF composites, and MOFs as supports, and highlight some instructive work.

6.1 Monometallic MOFs

In 2012, Mao *et al.* reported the first MOF material Cu-bipy-BTC with a block morphology for electrocatalytic ORR applications (Fig. 8a), which achieved an oxygen reduction process close to the ideal four-electron process in 0.1 M PBS (Fig. 8b).[87] This work develops a novel reference of MOF materials for the electrocatalytic ORR, which is

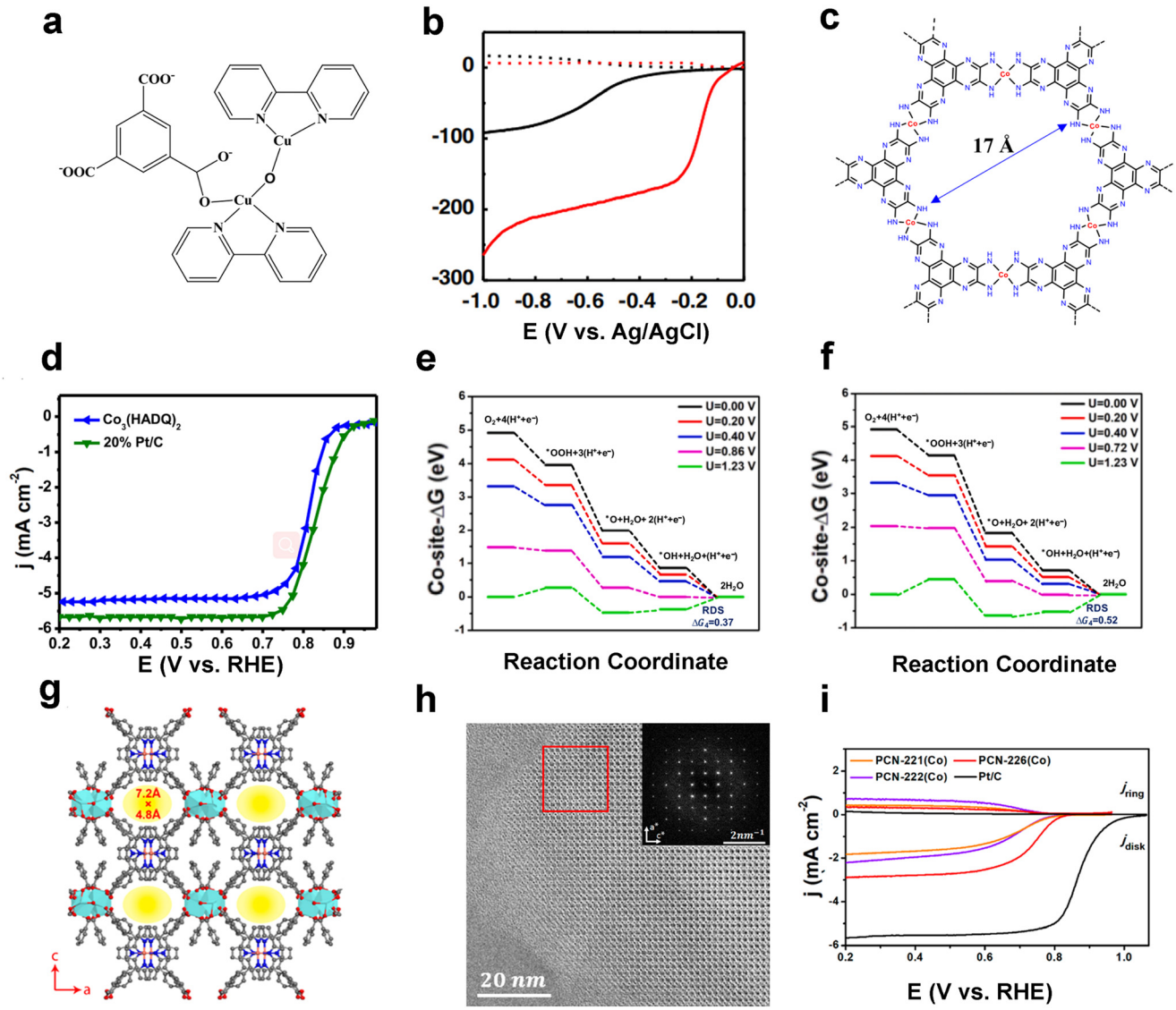

Fig. 8 MOF-based ORR electrocatalysts. (a) Coordination structure of copper atoms in Cu-bipy-BTC; (b) LSV curves of GC electrodes (solid curve), Pt ring electrodes (dotted curve), bare (black curve) and Cu-bipy-BTC-modified (red curve) in 0.1 M PBS. Rotation rate: 400 rpm. Reproduced with permission.[87] Copyright 2012, Elsevier; (c) structure of $Co_3(HADQ)_2$ MOF; (d) LSV curves of $Co_3(HADQ)_2$ MOF and Pt/C(20%) for ORR tests in 0.5 M H_2SO_4. Rotation rate: 1600 rpm. Calculated ORR free energy diagrams of $Co_3(HADQ)_2$ at different potentials on (e) the Co-site and (f) the pyridine N-site. Reproduced with permission.[88] Copyright 2022, Elsevier; (g) the crystal structure of PCN-226 was observed along the *b*-axis with an open window size of 7.2 Å × 4.8 Å; (h) HRTEM image of PCN-226(Cu), inset shows the Fourier transform of the image; (i) LSV curves of $Co_3(HADQ)_2$ MOF and Pt/C(20%) for ORR tests in 0.1 M KOH. Rotation rate: 1600 rpm. Reproduced with permission.[89] Copyright 2020, American Chemical Society.

environmentally friendly, cost effective, simple to synthesize, and expands the application of MOF materials in electrocatalysis. The strategy of constructing conductive nanosheet MOFs to enhance the performance is also applicable to facilitate electrocatalytic oxygen reduction reactions. In 2022, Zhao *et al.* designed a new two-dimensional MOF $Co_3(HADQ)_2$ with an ultra-high conductivity of 8385.744 S m^{-1} (Fig. 8c). $Co_3(HADQ)_2$ exhibits excellent ORR performance with a half-wave potential ($E_{1/2}$) of 0.825 V (V *vs.* RHE) in 0.5 M H_2SO_4 (Fig. 8d),[88] while having a number of transferred electrons close to that of a four-electron transfer process (n = 3.93). The Tafel slope of

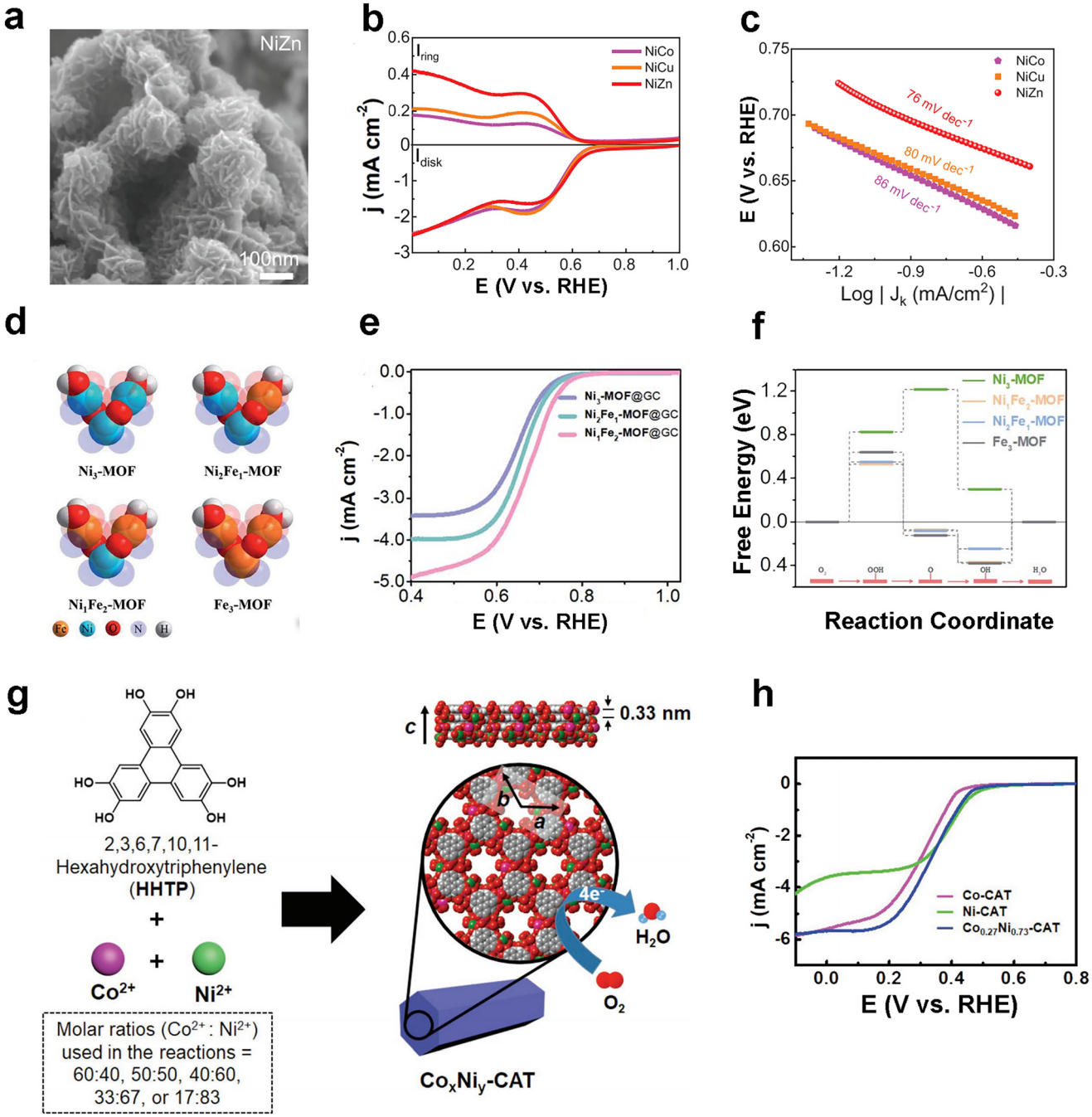

Fig. 9 MOF-based ORR electrocatalysts. (a) SEM images of NiZn MOF; (b) LSV curves and (c) Tafel slope of NiM MOF for ORR tests in O_2-saturated 0.1 M KOH. Rotation rate: 1600 rpm. Reproduced with permission.[90] Copyright 2022, Wiley-VCH; (d) visual representation of the established V-shaped trinuclear clusters; (e) LSV curves of Ni_1Fe_2-MOF@GC and other samples for ORR tests in O_2-saturated 0.1 M KOH, rotation rate: 2500 rpm; (f) calculated free energy diagram of the ORR of Ni_1Fe_2-MOF and other samples at 1.23 V. Reproduced with permission.[91] Copyright 2021, The Royal Society of Chemistry; (g) schematic diagram of the construction of bimetallic 2D MOF Co_xNi_y-CATs for the ORR; (h) LSV curves of $Co_{0.27}Ni_{0.73}$-CAT and other samples for ORR tests in O_2-saturated 0.1 M $NaClO_4$ and 0.02 M PBS, rotation rate: 1600 rpm. Reproduced with permission.[92] Copyright 2019, Wiley-VCH.

$Co_3(HADQ)_2$ is 79 mV dec^{-1}, slightly higher than that of Pt/C (76 mV dec^{-1}) and many electrocatalysts that have been reported (Table 1). It also has an excellent stability of only 5.4% loss after more than 20 000 CV cycles. Not only Co but also the Co–N_4 structure in $Co_3(HADQ)_2$ can be used as the active site of the ORR. In order to determine the true reflective active site of the ORR, the authors employed DFT to calculate the free energy changes of each basic step of the ORR at different potentials for the Co site and pyridine N site (Fig. 8e and f), and combined it with Bader charge analysis to confirm that the Co-site is the true active site for the ORR to occur.

Huang *et al.* designed the new highly stable Zr-based MOF PCN-226 based on the HSAB theory,[89] in which the authors introduced metalloporphyrin with oxygen reduction catalytic activity into the framework. The crystal structure of PCN-226 is shown in Fig. 8g, which possesses 7.2 Å × 4.8 Å pores. The arrangement of rectangular pores was confirmed by HRTEM characterization (Fig. 8h), which is consistent with the structural model. Exquisitely designed PCN-226 exhibited great ORR performance. PCN-226 possesses an onset potential of 0.83 V and a half-wave potential of 0.75 V (Fig. 8i). The strategy of this work is to improve the ORR kinetics by designing a highly stable Zr-MOF in which catalytically active ligands are introduced in high density, which contributes to the design of electrocatalysts for green energy conversion and storage.

6.2 Bimetallic MOFs

Since bimetallic MOFs have been widely used in the OER, the researchers speculate that the rational design of the structure of bimetallic MOFs can also play a role in improving their electrocatalytic oxygen reduction performance, considering

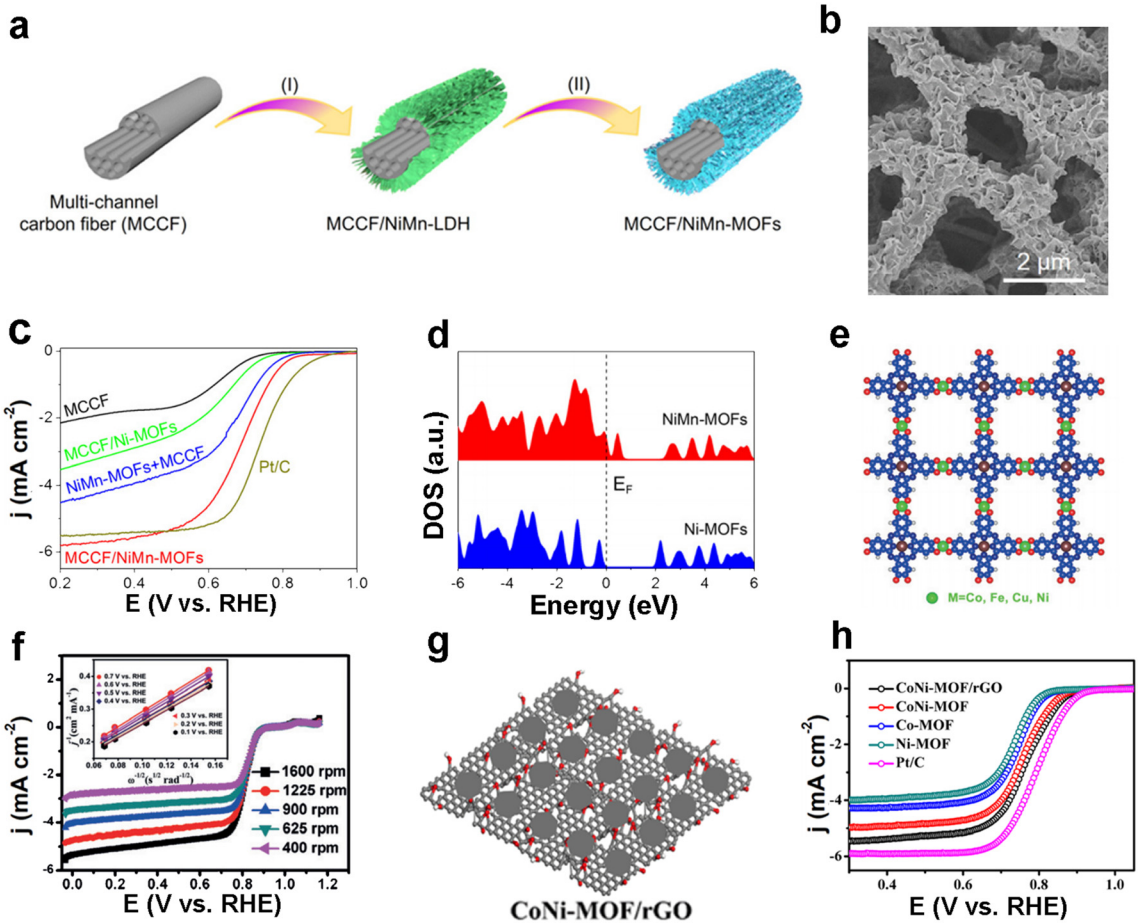

Fig. 10 MOF-based ORR electrocatalysts. (a) The synthesis process of MCCF (multi-channel carbon fiber)/NiMn-MOFs is illustrated by I) hydrothermal reaction to form MCCF/NiMn-LDH and II) conversion to MCCF/NiMn-MOFs by subsequent ligand exchange; (b) SEM images of MCCF/NiMn-MOFs; (c) LSV curves of MCCF/NiMn-MOFs and other samples for ORR tests in O_2-saturated 0.1 M KOH. Rotation rate: 1600 rpm; (d) calculated density of states (DOS) for Ni-MOFs and NiMn-MOFs. Reproduced with permission.[94] Copyright 2020, Wiley-VCH; (e) schematic diagram of the structure of PcCu–O_8–M (oxygen, carbon, hydrogen, copper and metal atoms are shown in red, blue, white, brown and green, respectively); (f) LSV curves of PcCu–O_8–Co/CNT at different rotating speeds for ORR tests in O_2-saturated 0.1 M KOH (the inset shows the corresponding K–L plots of PcCu–O_8–Co/CNT). Reproduced with permission.[95] Copyright 2019, Wiley-VCH; (g) schematic diagram of the CoNiMOF/rGO catalyst; (h) LSV curves of CoNi-MOF/rGO and other samples for ORR tests in O_2-saturated 0.1 M KOH. Rotation rate: 1600 rpm.[91] Reproduced with permission.[96] Copyright 2019, American Chemical Society.

that the oxygen reduction reaction is the inverse reaction of the oxygen evolution reaction. This subsection will summarize the representative work on bimetallic MOFs for the ORR in recent years. In 2022, Liu and co-workers explored the catalytic effect of Ni–M (M = Co, Cu, Zn)-based bimetallic MOFs in electrocatalytic oxygen reduction using a simple one-pot wet chemistry approach design.[90] The as-prepared NiZn MOF with a morphology of nanoparticles around 200 nm in diameter (Fig. 9a) exhibited excellent performance with up to 90% selectivity for H_2O_2 in the ORR process (Fig. 9b), significantly better than the NiCo MOF (45%) and NiCu MOF (55%), while having a low Tafel slope of 76 mV dec^{-1} (Fig. 9c). The authors used synchrotron radiation-Fourier transform infrared (SR-FTIR) spectroscopy and X-ray absorption fine structure (XAFS) techniques to reveal the generation of the key *OOH intermediate. It is also concluded that the high-valent $Ni^{(2+\delta)+}$ is the active site, which in turn optimizes the two-electron ORR process. Huang *et al.* designed MOFs with V-shaped trinuclear clusters as metal nodes (Fig. 9d), and Ni_1Fe_2-MOF@GC obtained by dropping a MOF on top of a glassy carbon electrode (GCE) demonstrated the trifunctional catalytic activity of the HER, OER and ORR.[91] For the ORR, the half-wave potential ($E_{1/2}$) of Ni_1Fe_2-MOF@GC was 0.676 V with an onset potential of 0.802 V and a limiting current density of 5.02 mA cm^{-2} (Fig. 9e). By Koutecky–Levich (K–L) equation analysis, only Ni_1Fe_2-MOF@GC is close to the theoretical value of 4.00, indicating that it achieves the full $4e^-$ ORR pathway. The authors calculated the free energy of the ORR step by DFT, and the ΔG value of the decisive speed step for Ni_1Fe_2-MOF is lower than that of Ni_3-MOF, Fe_3-MOF and Ni_2Fe_1-MOF, which laterally confirms and explains the experimental phenomenon.

Oh's group constructed bimetallic conducting 2D MOFs (Co_xNi_y-CATs) by a hydrothermal method using 2,3,6,7,10,11-hexahydroxytriphenylene (HHTP) and divalent metal ions (*e.g.* Co^{2+}, Ni^{2+} or Cu^{2+}) as building blocks through a strategy of constructing 2D conducting MOFs (Fig. 9g).[92] The reasonably controlled ratio of bimetallic $Co_{0.27}Ni_{0.73}$-CATs demonstrated better ORR performance than monometallic Co-CAT and Ni-CAT (Fig. 9h), further demonstrating the advantages of constructing bimetallic MOFs.

6.3 MOF-based composites

The strategy of compositing MOFs with inorganic/organic functional materials is equally feasible and efficient in electrocatalytic oxygen reduction.[93] Lou *et al.* successfully composited nickel–manganese-based bimetallic organic framework (NiMn-MOF) nanosheets with multichannel carbon fibers (MCCFs) with the help of a hydrothermal method and ligand exchange strategy (Fig. 10a).[94] The obtained MCCF/NiMn-MOFs with a single sheet thickness of about 40 nm in wrinkled morphology (Fig. 10b) showed excellent ORR catalytic performance. The half-wave potential of MCCF/NiMn-MOFs was 0.73 V and the TOF value was 0.17 s^{-1} at 0.5 V (Fig. 10c). Meanwhile, the number of transferred electrons was calculated to be 3.86 according to the K–L equation, which was close to the ideal four-electron transfer process. The authors performed DFT theoretical calculations and the density of states (DOS) plots revealed the presence of free electrons upon the addition of Mn nodes (Fig. 10d).

Combined with other calculations, they confirmed that the strong synergistic effect of Ni and Mn nodes makes NiMn-MOFs possess fast ORR kinetics. Moreover, Feng's group used 2,3,9,10,16,17,23,24-octahydroxy copper phthalocyanine (PcCu-$(OH)_8$) as a building block and constructed two-dimensional conjugated MOF PcCu–O_8–Co based on phthalocyanine using a solvothermal method (Fig. 10e), which was composited with carbon nanotubes to prepare PcCu–O_8–Co/CNTs with outstanding ORR activity in alkaline media ($E_{1/2}$ = 0.83 V, n = 3.93, j_L = 5.3 mA cm^{-2}) (Fig. 10f).[95]

To improve the electrical conductivity and catalytic properties of MOFs, compounding with conducting substrates such as reduced graphene oxide (rGO) and constructing two-dimensional nanosheets are very effective strategies. Previously in 2013, Loh *et al.* achieved trifunctional (HER, OER and ORR) catalytic effects using MOFs compounded with graphene oxide.[76] In 2019, Zhong's group constructed bimetallic CoNi-MOF nanosheets with rGO composite electrocatalysts (Fig. 10g).[96] As-prepared CoNi-MOF/rGO possesses excellent catalytic activity and stability. In 0.1 M KOH, CoNi-MOF/rGO has an onset overpotential (0.88 V) about 40 mV smaller than that of Pt/C and a low Tafel slope of 67 mV dec^{-1}, which is slightly higher than that of 56 mV dec^{-1} for Pt/C (Fig. 10h). The authors also assembled Zn–air cells using CoNi-MOF/rGO as an air electrode, which showed good energy density as well as cycling stability.

6.4 MOFs as supports

Suh and co-workers supported CuS nanoparticles with different contents onto non-conductive Cu-MOFs ($[Cu_3(BTC)_2$–$(H_2O)_3]$ (BTC = 1,3,5-benzenetricarboxylate)) (Fig. 11a and b).[97] The conductivity of the material after supporting CuS was increased 109 times compared to the pristine Cu-BTC. For the ORR, CuS(28 wt%)@Cu-BTC has an onset potential of 0.91 V (Fig. 11c), a transfer electron number of 3.82 (close to four-electron transfer), and a kinetic current density of 11.3 mA cm^{-2} at 0.55 V, achieving performance beyond that of the pristine MOF as well as nano-CuS, confirming the feasibility of the loaded nanoparticle strategy as well as providing design ideas for MOF-based ORR electrocatalysts. In 2021, Cao's group prepared Co porphyrin molecule@ZIF-8 composites (1@ZIF-8) by grafting porphyrin molecule catalysts onto the surface of MOF materials through ligand exchange using MOFs as supports (Fig. 11d).[98] In O_2-saturated 0.1 M KOH, 1@ZIF-8 (53 mV dec^{-1}) achieved a better Tafel slope than Pt/C (66 mV

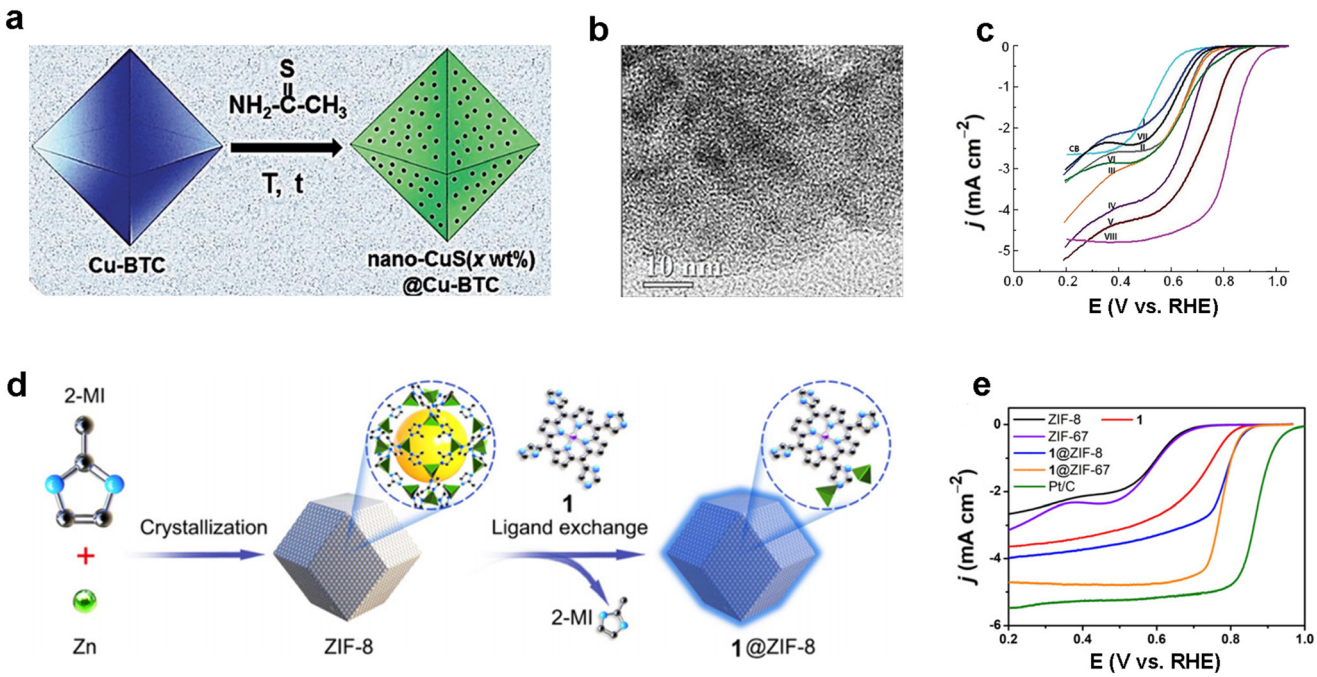

Fig. 11 MOF-based ORR electrocatalysts. (a) Schematic diagram of the synthesis of CuS(*x* wt%)@Cu-BTC nanoparticles; (b) TEM images of nano-CuS(28 wt%)@Cu-BTC; (c) LSV curves of nano-CuS(28 wt%)@Cu-BTC and other samples for ORR tests in O_2-saturated 0.1 M KOH, rotation rate: 1600 rpm. Reproduced with permission.[97] Copyright 2016, Wiley-VCH; (d) schematic diagram of the preparation of 1@ZIF-8; (e) LSV curves of 1@ZIF-8 and other samples for ORR tests in O_2-saturated 0.1 M KOH, rotation rate: 1600 rpm. Reproduced with permission.[98] Copyright 2021, Wiley-VCH.

dec^{-1}), demonstrating a more rapid ORR kinetics. Also, the porphyrin molecule grafted MOF achieved better half-wave potentials than the ungrafted porphyrin molecule material (Fig. 11e), confirming the effectiveness of the strategy. This work selects MOF supports with catalytic activity, realizes the synergistic catalytic effect of MOF supports and loadings, and jointly regulates the catalytic activity and selectivity of electrocatalysts, providing a fresh viewpoint for electrocatalysis and battery-related energy conversion applications.

The periodically arranged structure and the inherent porosity of MOFs make them outstanding candidates for electrocatalytic oxygen reduction reactions. More and more strategies are being used to enhance the conductivity of MOFs, such as the construction of conductive 2D MOFs and the *in situ* growth of 2D MOFs on conductive substrates, both of which would greatly facilitate the reaction kinetics of the ORR process. Meanwhile, MOF composites made with inorganic functional materials such as MXene confer overall higher electrocatalytic activity and stability. The stronger the ligand bond connection between the metal and ligand in MOFs, the more stable the MOFs may be, so the selection of strong metal–ligand bonds is necessary, and in addition, the selection of more redox active ligands may also contribute to the occurrence of the ORR. Considering the important role of the oxygen reduction reaction in metal–air cells as well as fuel cells, resource-rich and economical rare earth metal-based MOFs can be selected, which will be beneficial to solve the current situation of severe global fossil fuel consumption.

7 MOF-based electrocatalysts for the nitrogen reduction reaction

Ammonia is vital to human production and plays an important role in fertilizer production and clean energy applications.[100] Currently, ammonia is synthesized industrially mainly by the Haber–Bosch process, but the reaction conditions are harsh, requiring high temperatures (>673 K) and pressures (>700 bar), and are very energy intensive (about 1–2% of all human energy consumption). It also contributes to the emission of greenhouse gases such as CO_2, which leads to climate change such as acid rain and environmental damage.[101,102] Therefore, the development of an efficient, green and sustainable ammonia synthesis technology at room temperature is of epoch-making importance. In recent years, ammonia synthesis by the electrocatalytic nitrogen reduction reaction has received great attention due to its advantages of mild reaction conditions and wide sources of raw materials H_2O and N_2.[103] Based on this, this section will introduce MOF-based NRR electrocatalysts in the reaction mechanism, outline the development of current electrocatalytic nitrogen reduction electrocatalysts, and provide a reasonable outlook on the challenges and prospects of this emerging field.

The electrochemical nitrogen reduction reaction (NRR) is a six-electron transfer reaction, and the more widely accepted reaction steps are the following three steps: 1. adsorption and activation of nitrogen molecules, 2. progressive hydrogenation of activated N_2, and 3. desorption of NH_3.

Based on the hydrogenation and bond-breaking modes of N_2, there are two different reaction mechanisms for the reduction of nitrogen to ammonia: dissociative and associative mechanisms. In the dissociative mechanism, the N≡N bond is broken before the hydrogenation reaction, and the catalyst surface adsorbs individual nitrogen atoms, which are converted to NH_3 by the hydrogenation process. In the associative mechanism, the nitrogen molecule is hydrogenated while the two nitrogen atoms remain bound to each other, and there are two possible hydrogenation pathways: one is that the hydrogenation reaction occurs preferentially on the nitrogen atom farthest from the surface (assuming that the N_2 molecule is in the terminal coordination mode). Another hydrogenation pathway is that the nitrogen atoms of the two nitrogen centers are hydrogenated individually in turn until one of the nitriles is converted to NH_3 and the N≡N bond is broken.

Among them, since the dissociation energy of the N≡N triple bond is as high as 941 kJ mol^{-1} at room temperature and pressure, a large amount of energy is required for this process, leading to difficult activation and breakage, which in turn makes the NRR difficult to occur kinetically and thermodynamically. Also, the presence of competing hydrogen evolution reactions (HERs) leads to a significant

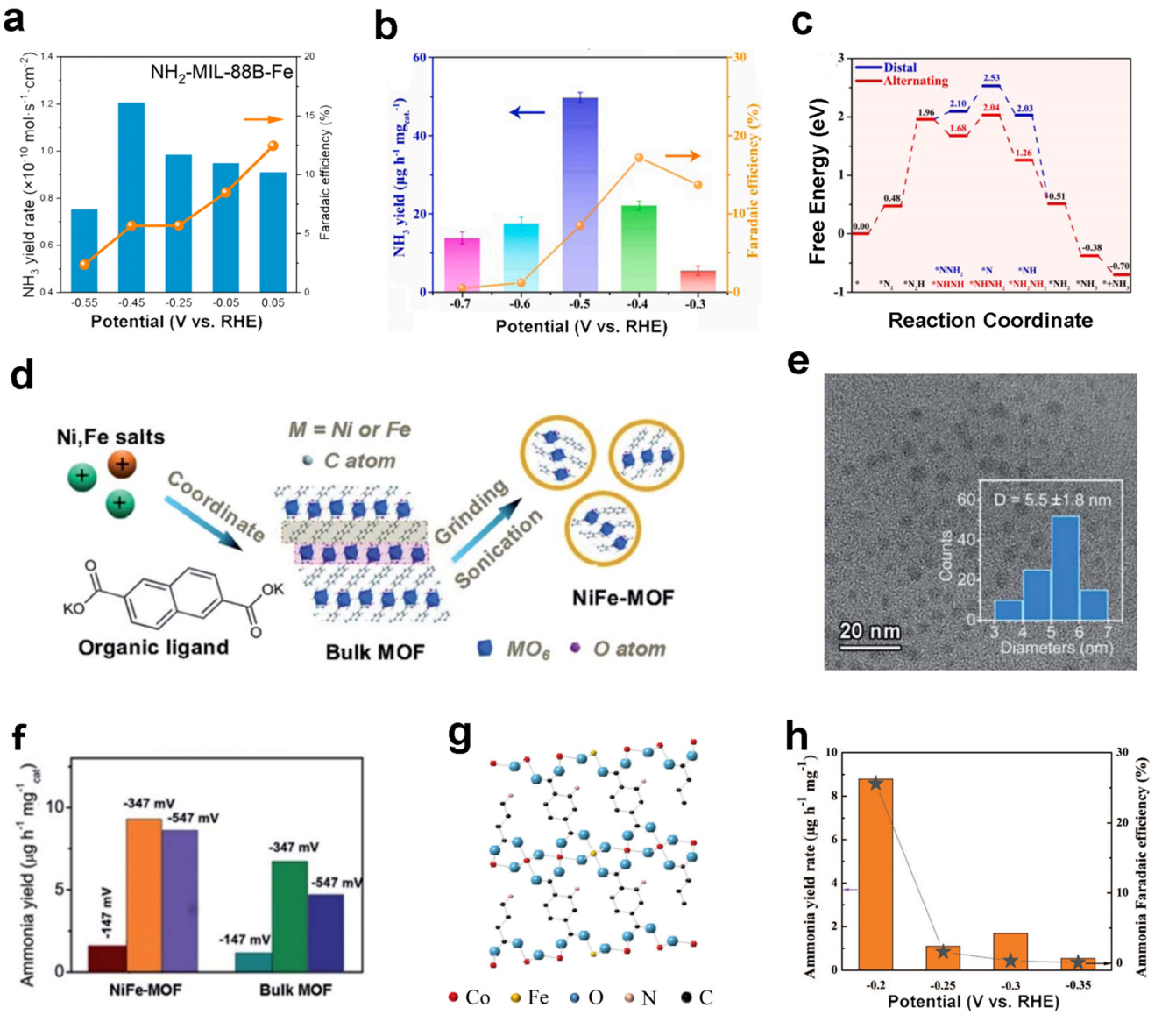

Fig. 12 MOF-based NRR electrocatalysts. (a) NH_3 yield and faradaic efficiency of NH_2-MIL-88B-Fe at each given potential. Reproduced with permission.[90] Copyright 2020, Springer Nature; (b) NH_3 yield and faradaic efficiency of OPA-PCN-222(Fe) at each given potential; (c) calculated free energy diagram of OPA-PCN-222(Fe) for the NRR. Reproduced with permission.[106] Copyright 2022, Elsevier; (d) schematic diagram of the preparation of NiFe-MOF; (e) high magnification TEM image of NiFe-MOF, and the inset shows the particle size distribution histogram; (f) NH_3 yield of NiFe-MOF at each given potential. Reproduced with permission.[107] Copyright 2020, The Royal Society of Chemistry; (g) crystal structure of Co_3-Fe-MOF; (h) NH_3 yield and faradaic efficiency of Co_3Fe-MOF at each given potential. Reproduced with permission.[108] Copyright 2020, The Royal Society of Chemistry.

decrease in NRR selectivity. Hence it is momentous to design NRR electrocatalysts with high activity and selectivity as well as stability.

7.1 Monometallic MOFs

To date, some monometallic MOFs have been applied to the NRR field. In 2017, Chen *et al.* first reported Fe, Co, and Cu-based MOFs, with the highest NH_3 yield (2.12×10^{-9} mol s^{-1} cm^{-2}) for the Fe-based MOF at 1.2 V and a Faraday efficiency value of 1.43%. In 2020, Li *et al.*[104] designed amino-functionalized monometallic iron-based MOF NH_2-MIL-88B-Fe with an ammonia yield of 1.205×10^{-10} mol s^{-1} cm^{-2} at room temperature and pressure in 0.1 M Na_2SO_4 (Fig. 12a), which was better than that of the non-amino-modified MIL-88B-Fe (3.575×10^{-11} mol s^{-1} cm^{-2}). Moreover, the Faraday efficiency of NH_2-MIL-88B-Fe at 0.05 V was 12.45%. In another study, Liu *et al.* used the classical HKUST-1 as an NRR electrocatalyst.[105] In a neutral 0.1 M Na_2SO_4 electrolyte, HKUST-1 gave a high ammonia yield of 46.63 μg h^{-1} mg_{cat}^{-1} at −0.75 V with an FE of 2.45%. However, the stability of HKUST-1 was poor, leading to the conversion of Cu(II) into Cu(I) during the NRR.

In the recent research of Du *et al.*, the hydrophobic molecule OPA (*n*-octadecylphosphonic acid) modified PCN-222(Fe) was constructed based on the fact that metalloporphyrin has been widely applied as a catalytic center for a variety of electrocatalytic reactions.[106] The optimal NH_3 yield and FE of OPA-PCN-222(Fe) were obtained by tuning hydrophobicity in 0.1 M HCl to optimize 49.7 μg h^{-1} mg_{cat}^{-1} (at −0.5 V) and 17.2% (at −0.4 V), respectively (Fig. 12b). The authors utilized DFT theoretical calculations to reveal the response mechanism of the NRR. The alternate pathway (red in Fig. 12c) requires less energy than the distal pathway (blue in Fig. 12c), so the former is applicable to the NRR process in this work. This work opens a new way of thinking for other researchers by tuning hydrophobicity to precisely optimize the NRR catalytic performance.

7.2 Bimetallic MOFs

The synergy between the two metal nodes in bimetallic MOFs and between the metal nodes and organic bridging ligands will be decisive for functionalized applications. Zhao and co-workers constructed a zero-dimensional bimetallic NiFe-MOF electrocatalyst with a nanoparticle diameter around 5.5 nm,

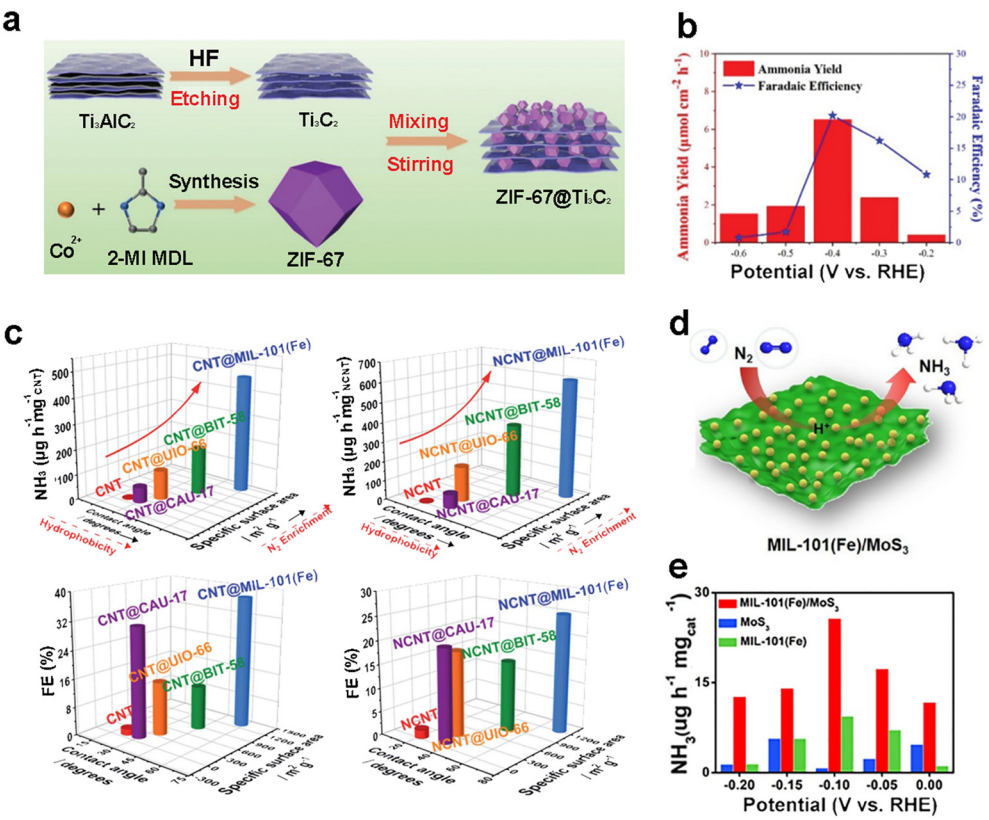

Fig. 13 MOF-based NRR electrocatalysts. (a) Schematic diagram of the synthesis of the ZIF-67@Ti_3C_2 composite; (b) NH_3 yield and faradaic efficiency of the ZIF-67@Ti_3C_2 composite at each given potential. Reproduced with permission.[111] Copyright 2021, The Royal Society of Chemistry; (c) optimal catalytic results of NRR catalysts obtained by adjusting the water contact angle and specific surface area. Reproduced with permission.[109] Copyright 2021, The Royal Society of Chemistry; (d) schematic diagram of the NRR process of MIL-101(Fe)/MoS_3; (e) comparison of the NH_3 yield of MIL-101(Fe)/MoS_3, MoS_3 and MIL-101(Fe) at each given potential. Reproduced with permission.[110] Copyright 2022, Springer Nature.

such a small MOF facilitates nitrogen activation and thus maximizes the metal active sites (Fig. 12d and e).[107] The ammonia yields of the NiFe-MOF were 9.3 μg h^{-1} mg_{cat}^{-1} with 11.5% FE in 0.1 M $NaHCO_3$ (Fig. 12f). The authors took advantage of DFT theoretical calculations to reveal that the constructed NiFe bimetallic MOF can synergistically suppress the energy barrier of the first ammonia synthesis step, significantly reducing the Gibbs free energy and thus optimizing the nitrogen reduction reaction process. This low-cost and easily prepared bimetallic MOF catalyst has great potential for applications in nitrogen fixation, electrochemical sensing, *etc.* Furthermore, Yan *et al.* designed Co_xFe-MOF nanosheets (10 nm thickness) by constructing a two-dimensional conducting bimetallic MOF.[108]

The authors coated the material on a glassy carbon electrode to evaluate the NRR performance. In an alkaline medium (0.1 M KOH), the NH_3 yield and the FE of the Co_3Fe-MOF were 8.79 μg h^{-1} mg_{cat}^{-1} and 25.64% (at −0.2 V), respectively. This work confirms the feasibility of the strategy of constructing two-dimensional bimetallic MOFs in the field of nitrogen reduction, while the Co_3Fe-MOF is also catalytically effective in the field of the OER, further offering a reference of bifunctional catalysts for the OER and NRR.

7.3 MOF-based composite

In 2021, Liu and co-workers constructed ZIF-67@Ti_3C_2 composites by growing ZIF-67 *in situ* on Ti_3C_2 MXene substrates (Fig. 13a),[109] effectively exploiting the advantages of high porosity and high specific surface area of the MOF and high conductivity of the MXene. The prepared ZIF-67@Ti_3C_2 composites showed great NRR performance at −0.4 V with NH_3 yields and Faraday efficiencies of 6.52 μmol h^{-1} cm^{-2} and 20.2%, respectively (Fig. 13b), which were superior to those of the pure MXene substrate and pure ZIF-67, confirming the superiority of the composite inorganic material strategy. In another study, Ding and co-workers designed CNTs and NCNTs to be composited with UiO-66.[110] The introduction of MOFs increased the water contact angle and N_2 uptake, resulting in enrichment of nitrogen concentration and suppression of HER competition (Fig. 13c). This work provides insight into the inhibition of the HER to promote the NRR and thus design efficient NRR electrocatalysts. In a recent study by Lang's group, MIL-101(Fe)/MoS_3 composites were rationally designed with the morphology of MoS_3 nanosheets loaded with ultra-small MIL-101(Fe) nanoparticles (Fig. 13d) (diameter of about 140

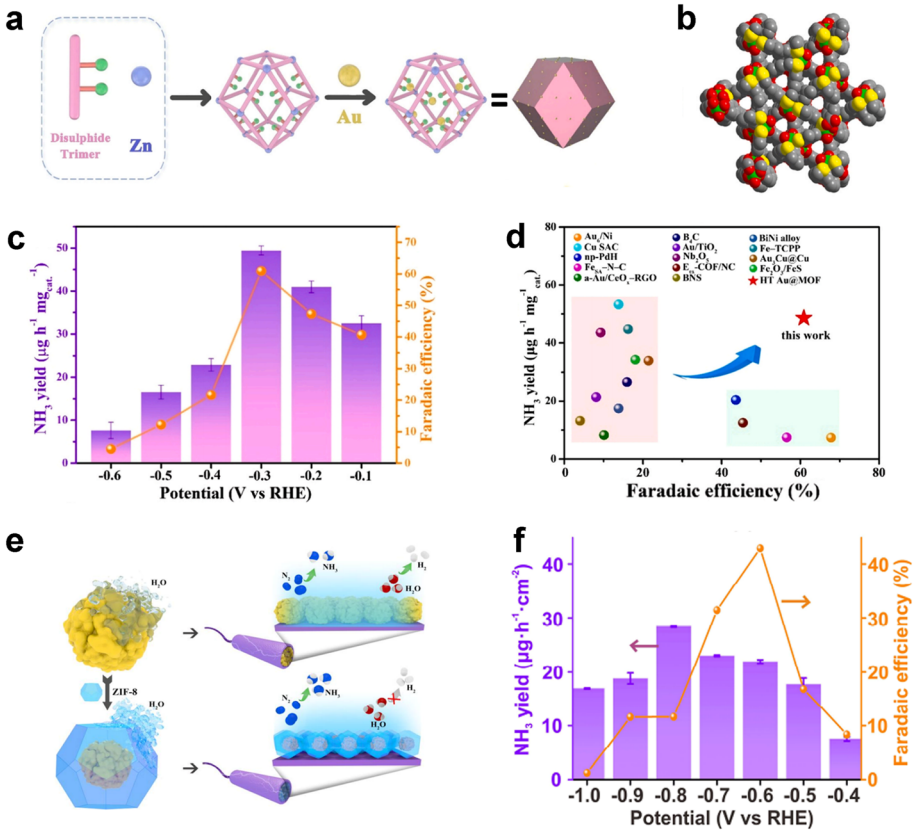

Fig. 14 MOF-based NRR electrocatalysts. (a) Schematic diagram of the synthesis of HT Au@MOF; (b) the three-dimensional crystal structure of the Zn-MOF; (c) NH_3 yield and faradaic efficiency of HT Au@MOF at each given potential; (d) comparison of the NH_3 yield and faradaic efficiency of HT Au@MOF with the reported NRR electrocatalysts.[107] Reproduced with permission.[112] Copyright 2022, Elsevier; (e) facilitation of nitrogen reduction by the NPG@ZIF-8 electrocatalyst; (f) NH_3 yield and faradaic efficiency of the NPG@ZIF-8 composite at each given potential.[108] Reproduced with permission.[113] Copyright 2019, Wiley-VCH.

nm).[111] Meanwhile, the ultra-small particles of MIL-101(Fe) show a highly crystalline state. For the NRR, the ammonia yield and Faraday efficiency of the MIL-101(Fe)/MoS_3 composites were 25.7 μg h^{-1} mg_{cat}^{-1} and 36.71% at −0.1 V, respectively (Fig. 13e), which were much better than those of pure MIL-101(Fe) and pure MoS_3 and most of the reported MOF-based NRR catalysts (Table 1).

7.4 MOFs as supports

Supporting nanoparticles with excellent electrocatalytic NRR properties into MOF materials with high porosity and large specific surface area is one of the methods to design efficient NRR catalysts. Du and co-workers constructed a MOF featuring disulfide trimers to confine gold nanoparticles (Fig. 14a).[112] And hydrophobic silicone was designed on the surface of the Au@MOF, which further enhanced the electrocatalytic NRR performance. In detail, MOFs based on disulfide trimers were synthesized *via* the coordination assembly of Zn(II) cations and dicarboxylic ligands with thiol groups (Fig. 14b). Surprisingly, the optimized HT Au@MOF exhibits an outstanding NH_3 yield of 49.5 μg h^{-1} mg_{cat}^{-1} (Fig. 14c) and shows one of the best Faraday efficiencies (60.9%, Fig. 14d) of the current NRR catalysts (Table 1) at −0.3 V. Another study using the support nanoparticle strategy applied to the field of the NRR was reported in 2019.[113] An excellent ammonia yield (28.7 ± 0.9 μg h^{-1} cm^{-2}, at −0.6 V) and a remarkable Faraday efficiency (44%, at −0.8 V) were demonstrated using ZIF-8 embedded nanoporous gold particles using a three-electrode system in 0.1 M Na_2SO_4 (Fig. 14e and f). The brilliant NRR catalytic performance comes from the synergistic effect of the two components of gold nanoparticles and ZIF-8, as well as core–shell nanostructures. These two studies provide new ideas for MOF-supported nanoparticles, and the strategy of MOFs as supports will be further and widely developed in the future.

The above categorical enumeration proves that MOF-based materials are promising NRR electrocatalysts. Similar to other electrocatalytic reactions in the previous section, the strategy of compounding MOFs with active materials shows surprising results. At the same time, the pore tunability of the MOF itself is used to achieve better performance of encapsulated nanoparticles, which possess a faster mass transfer rate and better nitrogen permeability, providing excellent transport channels and thus accelerating electron transport, further significantly improving the catalytic activity of nitrogen ammonia synthesis. Furthermore, since the ammonia content in the air environment will contaminate the accuracy of ammonia detection to some extent, the quantitative detection method of ammonia synthesized by the electrocatalytic NRR in the future should be corroborated by using multiple indicators together, such as the Nessler method, the indophenol blue method, ion chromatography, the ^{15}N gas tracking method, *etc.* In addition, the study of the NRR mechanism should also be paid special attention. Finally, for industrial electrocatalytic nitrogen fixation, the stability of electrocatalysts should be emphasized more.

8 Conclusions and perspectives

MOFs have proven to be very promising electrocatalysts in the field of electrocatalysis because of their customizable structures, high porosity, high specific surface area and easy functionalization. In recent years, research on MOFs in electrocatalysis has undergone rapid development. In this review, we first summarize the parameters for evaluating electrocatalytic reactions, and then we summarize in detail the progress of MOF materials in different electrocatalytic reactions, including the hydrogen evolution reaction, hydrogen oxidation reaction, oxygen evolution reaction, oxygen reduction reaction, and nitrogen reduction reaction, categorized by monometallic MOFs, bimetallic MOFs, MOF-based composites, and MOFs as supports. Among them, the design modulation strategies of electrocatalysts are covered, such as the synthesis of two-dimensional conducting MOFs, the design of unsaturated metal sites, the construction of MOF nanoarrays and the selection of highly stable MOFs. Specific structures are precisely prepared on a micro/macro basis by several of these strategies to improve the conductivity, stability, and number of active sites of catalysts and to increase the intrinsic activity of individual active sites. In addition, the catalytic performance of various electrocatalytic reactions is summarized in a tabular format to visualize the catalytic performance. The reaction process and reaction mechanism of each electrocatalytic reaction are also summarized to provide the reader with a clearer and deeper understanding of each reaction. Although milestones have been achieved in the current performance level of MOF-based electrocatalysts, there are still gaps before industrial applications, and the following issues still need to be further explored and addressed.

First, there are few non-precious metal MOF catalysts that have achieved activity and stability beyond those of precious metal benchmark catalysts, both in the relatively well-developed HER, OER and ORR fields and in the nascent HOR and NRR fields. Meanwhile, the origin of the known kinetic slowness has not been explored, and the underlying basis needs to be explained by theoretical and experimental support. From an experimental point of view, *in situ* monitoring and characterization are strongly recommended to gain insight into the ligand structure and pore channel alterations occurring in MOFs during the catalytic process, as well as to observe the changes, interactions and band intensities of each catalytic reaction intermediate in real time, such as *in situ* XPS/Raman/PXRD spectroscopy/patterns, which can help to reveal the true reaction process of electrocatalysis. In addition, density functional theory (DFT) calculations are an important tool to determine the optimal free energy active site and to corroborate the experimental phenomena. Further, theoretical calculations can also be applied to guide the design of MOF catalysts. Although many researchers are now digging deeper into theoretical

calculations for experimental predictions, a reasonable combination of theoretical results and experiments still cannot be achieved every time and still needs to be systematically studied and explored by a large number of scholars.

Second, the microstructure of MOF-based electrocatalysts should be more precisely controlled. Electrocatalytic materials have high requirements for morphology, which determines the catalytic performance to a certain extent. The morphology with small nanoparticle size and uniform distribution is more favorable for charge transport. Furthermore, the synergistic effect between MOFs and complex species needs to be precisely tuned, which is one of the key factors affecting the catalytic performance. In addition, the conductivity of electrocatalysts is crucial for electrocatalytic reactions, and since MOFs themselves have poor conductivity, the conductivity and thus the catalytic activity can be largely improved by constructing two-dimensional conductive MOFs.

Third, MOFs are currently more prone to deactivation than inorganic active materials in various electrocatalytic reactions. Therefore, highly stable MOFs can be designed firstly based on HASB theory. And then, their stability can be improved by adjusting the microstructure, crystallinity and crystal orientation. Therefore, based on these difficult challenges and existing problems, researchers need to further develop economical, environmentally friendly and highly durable MOF-based electrocatalysts to facilitate industrial applications.

Conflicts of interest

There are no conflicts to declare.

Acknowledgements

The authors acknowledge the financial support from the National Natural Science Foundation of China (22035003 and 22201137), the Nature Science Fund of Tianjin, China (19JCZDJC37200), the Fundamental Research Funds for the Central Universities (63223020) and the Haihe Laboratory of Sustainable Chemical Transformations (YYJC202101).

Notes and references

1 H. Sun, C. Tian, G. Fan, J. Qi, Z. Liu, Z. Yan, F. Cheng, J. Chen, C. P. Li and M. Du, Boosting activity on Co_4N porous nanosheet by coupling CeO_2 for efficient electrochemical overall Water splitting at high current densities, *Adv. Funct. Mater.*, 2020, **30**, 1910596.

2 C. L. Fu, Y. Wang and J. H. Huang, Hybrid of quaternary layered double hydroxides and carbon nanotubes for oxygen evolution reaction, *Chin. J. Struct. Chem.*, 2020, **39**, 1807–1816.

3 Y. R. Wang, H. M. Ding, S. N. Sun, J. W. Shi, Y. L. Yang, Q. Li, Y. Chen, S. L. Li and Y.-Q. Lan, Light, heat and electricity Integrated energy conversion system: photothermal-assisted Co-electrolysis of CO_2 and methanol, *Angew. Chem., Int. Ed.*, 2022, **61**, e202212162.

4 Q. Huang, Q. Li, J. Liu, Y. R. Wang, R. Wang, L. Z. Dong, Y. H. Xia, J. L. Wang and Y.-Q. Lan, Disclosing CO_2 activation mechanism by hydroxyl-induced crystalline structure transformation in electrocatalytic process, *Matter*, 2019, **1**, 1656–1668.

5 Y. Zhang, J. Li, X. Yang, P. Zhang, J. Pang, B. Li and H. C. Zhou, A mesoporous NNN-pincer-based metal-organic framework scaffold for the preparation of noble-metal-free catalysts, *Chem. Commun.*, 2019, **55**, 2023–2026.

6 L. Yang, P. Cai, L. Zhang, X. Xu, A. A. Yakovenko, Q. Wang, J. Pang, S. Yuan, X. Zou, N. Huang, Z. Huang and H. C. Zhou, Ligand-directed conformational control over porphyrinic zirconium metal-organic frameworks for size-selective catalysis, *J. Am. Chem. Soc.*, 2021, **143**, 12129–12137.

7 G. Y. Qiao, S. Yuan, J. Pang, H. Rao, C. T. Lollar, D. Dang, J. S. Qin, H. C. Zhou and J. Yu, Functionalization of zirconium-based metal-organic layers with tailored pore environments for heterogeneous catalysis, *Angew. Chem., Int. Ed.*, 2020, **59**, 18224–18228.

8 O. M. Yaghi, G. Li and H. Li, Selective binding and removal of guests in a microporous metal–organic framework, *Nature*, 1995, **378**, 703–706.

9 J. Pang, M. Wu, J.-S. Qin, C. Liu, C. T. Lollar, D. Yuan, M. Hong and H.-C. Zhou, Solvent-assisted, thermally triggered structural transformation in flexible mesoporous metal–organic frameworks, *Chem. Mater.*, 2019, **31**, 8787–8793.

10 B. Li, Y. M. Zhao, A. Kirchon, J. D. Pang, X. Y. Yang, G. L. Zhuang and H. C. Zhou, Unconventional method for fabricating valence tautomeric materials: integrating redox center within a metal-organic framework, *J. Am. Chem. Soc.*, 2019, **141**, 6822–6826.

11 Q. Chen, S. Xian, X. Dong, Y. Liu, H. Wang, D. H. Olson, L. J. Williams, Y. Han, X.-H. Bu and J. Li, High-efficiency separation of n-hexane by a dynamic Metal-organic framework with reduced energy consumption, *Angew. Chem., Int. Ed.*, 2021, **60**, 10593–10597.

12 W.-G. Cui, T.-L. Hu and X.-H. Bu, Metal-organic framework materials for the separation and purification of light hydrocarbons, *Adv. Mater.*, 2020, **32**, 1806445.

13 X.-T. Liu, K. Wang, Z. Chang, Y.-H. Zhang, J. Xu, Y. S. Zhao and X.-H. Bu, Engineering donor-acceptor heterostructure metal-organic framework crystals for photonic logic computation, *Angew. Chem., Int. Ed.*, 2019, **58**, 13890–13896.

14 M.-H. Yu, B. Space, D. Franz, W. Zhou, C. He, L. Li, R. Krishna, Z. Chang, W. Li, T.-L. Hu and X.-H. Bu, Enhanced gas uptake in a microporous metal-organic framework via a sorbate induced-fit mechanism, *J. Am. Chem. Soc.*, 2019, **141**, 17703–17712.

15 Z. Di, C. Liu, J. Pang, C. Chen, F. Hu, D. Yuan, M. Wu and M. Hong, Cage-like porous materials with simultaneous high C_2H_2 storage and excellent C_2H_2/CO_2 separation performance, *Angew. Chem., Int. Ed.*, 2021, **60**, 10828–10832.

16 W. Q. Xu, S. He, C. C. Lin, X. J. Liu, L. C. Jiang and J. J. Jiang, MOF-derived Cu_2O/Cu NPs on N-doped porous carbon as a multifunctional sensor for mercury(II) and glucose with wide detection range, *Chin. J. Struct. Chem.*, 2020, **39**, 1522–1530.

17 L. J. Kong, M. Liu, H. Huang, Y. H. Xu and X. H. Bu, Metal/covalent-organic framework based cathodes for metal-ion batteries, *Adv. Energy Mater.*, 2022, **12**, 2100172.

18 J. He, N. Li, Z. G. Li, M. Zhong, Z. X. Fu, M. Liu, J. C. Yin, Z. Shen, W. Li, J. Zhang, Z. Chang and X. H. Bu, Strategic defect engineering of metal–organic frameworks for optimizing the fabrication of single-atom catalysts, *Adv. Funct. Mater.*, 2021, **31**, 2103597.

19 N. Li, Z. Chang, M. Zhong, Z.-X. Fu, J. Luo, Y.-F. Zhao, G.-B. Li and X.-H. Bu, Functionalizing MOF with redox-active tetrazine moiety for improving the performance as cathode of Li–O_2 batteries, *CCS Chem.*, 2021, **3**, 1297–1305.

20 L. Kong, M. Zhong, W. Shuang, Y. Xu and X.-H. Bu, Electrochemically active sites inside crystalline porous materials for energy storage and conversion, *Chem. Soc. Rev.*, 2020, **49**, 2378–2407.

21 W. Wang, X. Xu, W. Zhou and Z. Shao, Recent Progress in Metal-organic frameworks for applications in electrocatalytic and photocatalytic water splitting, *Adv. Sci.*, 2017, **4**, 1600371.

22 Z. Li, R. Gao, M. Feng, Y. P. Deng, D. Xiao, Y. Zheng, Z. Zhao, D. Luo, Y. Liu, Z. Zhang, D. Wang, Q. Li, H. Li, X. Wang and Z. Chen, Modulating metal–organic frameworks as advanced oxygen electrocatalysts, *Adv. Energy Mater.*, 2021, **11**, 2003291.

23 X. Liu, T. Yue, K. Qi, Y. Qiu, B. Y. Xia and X. Guo, Metal-organic framework membranes: from synthesis to electrocatalytic applications, *Chin. Chem. Lett.*, 2020, **31**, 2189–2201.

24 L. Jiao, Y. Wang, H. L. Jiang and Q. Xu, Metal-organic frameworks as platforms for catalytic applications, *Adv. Mater.*, 2018, **30**, 1703663.

25 Q. Wang and D. Astruc, State of the art and prospects in metal-organic framework (MOF)-based and MOF-derived nanocatalysis, *Chem. Rev.*, 2020, **120**, 1438–1511.

26 X. Xiao, L. Zou, H. Pang and Q. Xu, Synthesis of micro/nanoscaled metal-organic frameworks and their direct electrochemical applications, *Chem. Soc. Rev.*, 2020, **49**, 301–331.

27 A. Morozan and F. Jaouen, Metal organic frameworks for electrochemical applications, *Energy Environ. Sci.*, 2012, **5**, 9269–9290.

28 X. Long, J. Meng, J. Gu, L. Ling, Q. Li, N. Liu, K. Wang and Z. Li, Interfacial engineering of NiFeP/NiFe-LDH heterojunction for efficient overall water splitting, *Chin. J. Struct. Chem.*, 2022, **41**, 2204046–2204053.

29 H. Sun, Z. Yan, C. Tian, C. Li, X. Feng, R. Huang, Y. Lan, J. Chen, C. P. Li, Z. Zhang and M. Du, Bixbyite-type Ln_2O_3 as promoters of metallic Ni for alkaline electrocatalytic hydrogen evolution, *Nat. Commun.*, 2022, **13**, 3857.

30 Y. Zhao, X. Wang, Z. Li, P. Zhao, C. Tao, G. Cheng and W. Luo, Enhanced catalytic activity of Ru through N modification toward alkaline hydrogen electrocatalysis, *Chin. Chem. Lett.*, 2022, **33**, 1065–1069.

31 C.-P. Wang, L.-J. Kong, H. Sun, M. Zhong, H.-J. Cui, Y.-H. Zhang, D.-H. Wang, J. Zhu and X.-H. Bu, Carbon layer coated Ni_3S_2/MoS_2 nanohybrids as efficient bifunctional electrocatalysts for overall water splitting, *ChemElectroChem*, 2019, **6**, 5603–5609.

32 W. Zhao, B. Jin, L. Wang, C. Ding, M. Jiang, T. Chen, S. Bi, S. Liu and Q. Zhao, Ultrathin Ti_3C_2 nanowires derived from multi-layered bulks for high-performance hydrogen evolution reaction, *Chin. Chem. Lett.*, 2022, **33**, 557–561.

33 H. Sun, Z. Yan, F. Liu, W. Xu, F. Cheng and J. Chen, Self-supported transition-metal-based electrocatalysts for hydrogen and oxygen evolution, *Adv. Mater.*, 2020, **32**, 1806326.

34 J. Xu, G. Shao, X. Tang, F. Lv, H. Xiang, C. Jing, S. Liu, S. Dai, Y. Li, J. Luo and Z. Zhou, Frenkel-defected monolayer MoS_2 catalysts for efficient hydrogen evolution, *Nat. Commun.*, 2022, **13**, 2193.

35 J. C. McGlynn, T. Dankwort, L. Kienle, N. A. G. Bandeira, J. P. Fraser, E. K. Gibson, I. Cascallana-Matias, K. Kamaras, M. D. Symes, H. N. Miras and A. Y. Ganin, The rapid electrochemical activation of $MoTe_2$ for the hydrogen evolution reaction, *Nat. Commun.*, 2019, **10**, 4916.

36 S. Hu and W. X. Li, Sabatier principle of metal-support interaction for design of ultrastable metal nanocatalysts, *Science*, 2021, **374**, 1360–1365.

37 S. Yuan, L. Feng, K. Wang, J. Pang, M. Bosch, C. Lollar, Y. Sun, J. Qin, X. Yang, P. Zhang, Q. Wang, L. Zou, Y. Zhang, L. Zhang, Y. Fang, J. Li and H. C. Zhou, Stable metal-organic frameworks: design, synthesis, and applications, *Adv. Mater.*, 2018, **30**, 1704303.

38 Y. P. Wu, W. Zhou, J. Zhao, W. W. Dong, Y. Q. Lan, D. S. Li, C. Sun and X. Bu, Surfactant-assisted phase-selective synthesis of new cobalt MOFs and their efficient electrocatalytic hydrogen evolution reaction, *Angew. Chem., Int. Ed.*, 2017, **56**, 13001–13005.

39 H. Jin, C. Guo, X. Liu, J. Liu, A. Vasileff, Y. Jiao, Y. Zheng and S. Z. Qiao, Emerging two-dimensional nanomaterials for electrocatalysis, *Chem. Rev.*, 2018, **118**, 6337–6408.

40 C. Tan, X. Cao, X. J. Wu, Q. He, J. Yang, X. Zhang, J. Chen, W. Zhao, S. Han, G. H. Nam, M. Sindoro and H. Zhang, Recent advances in ultrathin two-dimensional nanomaterials, *Chem. Rev.*, 2017, **117**, 6225–6331.

41 B. Geng, F. Yan, X. Zhang, Y. He, C. Zhu, S. L. Chou, X. Zhang and Y. Chen, Conductive CuCo-based bimetal organic framework for efficient hydrogen evolution, *Adv. Mater.*, 2021, **33**, 2106781.

42 Y. Luo, X. Yang, L. He, Y. Zheng, J. Pang, L. Wang, R. Jiang, J. Hou, X. Guo and L. Chen, Structural and electronic modulation of iron-based bimetallic metal-organic framework bifunctional electrocatalysts for efficient overall water splitting in alkaline and seawater environment, *ACS Appl. Mater. Interfaces*, 2022, **14**, 46374–46385.

43 R. Z. Zhang, L. L. Lu, Z. H. Chen, X. Zhang, B. Y. Wu, W. Shi and P. Cheng, Bimetallic cage-based metal-organic frameworks for electrochemical hydrogen evolution reaction with enhanced activity, *Chem. – Eur. J.*, 2022, **28**, e202200401.

44 W. Cheng, H. Zhang, D. Luan and X. W. D. Lou, Exposing unsaturated Cu_1-O_2 sites in nanoscale Cu-MOF for efficient electrocatalytic hydrogen evolution, *Sci. Adv.*, 2021, **7**, eabg2580.

45 L. Wang, L. Song, Z. Yang, Y. M. Chang, F. Hu, L. Li, L. Li, H. Y. Chen and S. Peng, Electronic modulation of metal–organic frameworks by interfacial bridging for efficient pH-universal hydrogen evolution, *Adv. Funct. Mater.*, 2022, 2210322.

46 D. Zhu, J. Liu, Y. Zhao, Y. Zheng and S. Z. Qiao, Engineering 2D metal-organic framework/MoS_2 interface for enhanced alkaline hydrogen evolution, *Small*, 2019, **15**, 1805511.

47 L. Deng, F. Hu, M. Ma, S. C. Huang, Y. Xiong, H. Y. Chen, L. Li and S. Peng, Electronic modulation caused by interfacial Ni-O-M (M=Ru, Ir, Pd) bonding for accelerating hydrogen evolution kinetics, *Angew. Chem., Int. Ed.*, 2021, **60**, 22276–22282.

48 K. Rui, G. Zhao, M. Lao, P. Cui, X. Zheng, X. Zheng, J. Zhu, W. Huang, S. X. Dou and W. Sun, Direct hybridization of noble metal nanostructures on 2D metal-organic framework nanosheets to catalyze hydrogen evolution, *Nano Lett.*, 2019, **19**, 8447–8453.

49 S. Ji, Y. Chen, X. Wang, Z. Zhang, D. Wang and Y. Li, Chemical synthesis of single atomic site catalysts, *Chem. Rev.*, 2020, **120**, 11900–11955.

50 A. Wang, J. Li and T. Zhang, Heterogeneous single-atom catalysis, *Nat. Rev. Chem.*, 2018, **2**, 65–81.

51 C. Xia, Y. Qiu, Y. Xia, P. Zhu, G. King, X. Zhang, Z. Wu, J. Y. T. Kim, D. A. Cullen, D. Zheng, P. Li, M. Shakouri, E. Heredia, P. Cui, H. N. Alshareef, Y. Hu and H. Wang, General synthesis of single-atom catalysts with high metal loading using graphene quantum dots, *Nat. Chem.*, 2021, **13**, 887–894.

52 Y. Sun, Z. Xue, Q. Liu, Y. Jia, Y. Li, K. Liu, Y. Lin, M. Liu, G. Li and C. Y. Su, Modulating electronic structure of metal-organic frameworks by introducing atomically dispersed Ru for efficient hydrogen evolution, *Nat. Commun.*, 2021, **12**, 1369.

53 J. Zhou, Y. Dou, X. Q. Wu, A. Zhou, L. Shu and J. R. Li, Alkali-etched Ni(II)-based metal-organic framework nanosheet arrays for electrocatalytic overall water splitting, *Small*, 2020, **16**, 1906564.

54 F. Shahbazi Farahani, M. S. Rahmanifar, A. Noori, M. F. El-Kady, N. Hassani, M. Neek-Amal, R. B. Kaner and M. F. Mousavi, Trilayer metal-organic frameworks as multifunctional electrocatalysts for energy conversion and storage applications, *J. Am. Chem. Soc.*, 2022, **144**, 3411–3428.

55 M. Gu, S. C. Wang, C. Chen, D. Xiong and F. Y. Yi, Iron-based metal-organic framework system as an efficient bifunctional electrocatalyst for oxygen evolution and hydrogen evolution reactions, *Inorg. Chem.*, 2020, **59**, 6078–6086.

56 L. Zhang, S. Li, C. J. Gomez-Garcia, H. Ma, C. Zhang, H. Pang and B. Li, Two novel polyoxometalate-encapsulated metal-organic nanotube frameworks as stable and highly efficient electrocatalysts for hydrogen evolution reaction, *ACS Appl. Mater. Interfaces*, 2018, **10**, 31498–31504.

57 W. Zhou, Z. Xue, Q. Liu, Y. Li, J. Hu and G. Li, Trimetallic MOF-74 films grown on Ni foam as bifunctional electrocatalysts for overall water splitting, *ChemSusChem*, 2020, **13**, 5647–5653.

58 J. Duan, S. Chen and C. Zhao, Ultrathin metal-organic framework array for efficient electrocatalytic water splitting, *Nat. Commun.*, 2017, **8**, 15341.

59 W. Ni, T. Wang, F. Heroguel, A. Krammer, S. Lee, L. Yao, A. Schuler, J. S. Luterbacher, Y. Yan and X. Hu, An efficient nickel hydrogen oxidation catalyst for hydroxide exchange membrane fuel cells, *Nat. Mater.*, 2022, **21**, 804–810.

60 J. Li, S. Ghoshal, M. K. Bates, T. E. Miller, V. Davies, E. Stavitski, K. Attenkofer, S. Mukerjee, Z. F. Ma and Q. Jia, Experimental proof of the bifunctional mechanism for the hydrogen oxidation in alkaline media, *Angew. Chem., Int. Ed.*, 2017, **56**, 15594–15598.

61 Y. Men, X. Su, P. Li, Y. Tan, C. Ge, S. Jia, L. Li, J. Wang, G. Cheng, L. Zhuang, S. Chen and W. Luo, Oxygen-inserted top-surface layers of Ni for boosting alkaline hydrogen oxidation electrocatalysis, *J. Am. Chem. Soc.*, 2022, **144**, 12661–12672.

62 Y. Yang, X. Sun, G. Han, X. Liu, X. Zhang, Y. Sun, M. Zhang, Z. Cao and Y. Sun, Enhanced electrocatalytic hydrogen oxidation on Ni/NiO/C derived from a Nickel-based metal-organic framework, *Angew. Chem., Int. Ed.*, 2019, **58**, 10644–10649.

63 Q. Zhang, Y. Wang, Y. Wang, S. Yang, X. Wu, B. Lv, N. Wang, Y. Gao, X. Xu, H. Lei and R. Cao, Electropolymerization of cobalt porphyrins and corroles for the oxygen evolution reaction, *Chin. Chem. Lett.*, 2021, **32**, 3807–3810.

64 Q. Mou, X. Wang, Z. Xu, P. Zul, E. Li, P. Zhao, X. Liu, H. Li and G. Cheng, A synergy establishment by metal-organic framework and carbon quantum dots to enhance electrochemical water oxidation, *Chin. Chem. Lett.*, 2022, **33**, 562–566.

65 Q. Huang, Q. Niu, X.-F. Li, J. Liu, S.-N. Sun, L.-Z. Dong, S.-L. Li, Y.-P. Cai and Y.-Q. Lan, Demystifying the roles of single metal site and cluster in CO_2 reduction via light and electric dual-responsive polyoxometalate-based metal-organic frameworks, *Sci. Adv.*, 2022, **8**, eadd5598.

66 Z. Xin, Y.-R. Wang, Y. Chen, W.-L. Li, L.-Z. Dong and Y.-Q. Lan, Metallocene implanted metalloporphyrin organic framework for highly selective CO_2 electroreduction, *Nano Energy*, 2020, **67**, 104233.

67 W. Zheng, M. Liu and L. Y. S. Lee, Electrochemical instability of metal–organic frameworks: in situ spectroelectrochemical investigation of the real active sites, *ACS Catal.*, 2019, **10**, 81–92.

68 S. Zhao, C. Tan, C.-T. He, P. An, F. Xie, S. Jiang, Y. Zhu, K.-H. Wu, B. Zhang, H. Li, J. Zhang, Y. Chen, S. Liu, J. Dong and Z. Tang, Structural transformation of highly active metal–organic framework electrocatalysts during the oxygen evolution reaction, *Nat. Energy*, 2020, **5**, 881–890.

69 J.-T. Ren, C.-Y. Wan, T.-Y. Pei, X.-W. Lv and Z.-Y. Yuan, Promotion of electrocatalytic nitrogen reduction reaction on N-doped porous carbon with secondary heteroatoms, *Appl. Catal., B*, 2020, **266**, 118633.

70 C. Zhang, Q. Qi, Y. Mei, J. Hu, M. Sun, Y. Zhang, B. Huang, L. Zhang and S. Yang, Rationally reconstructed metal-organic frameworks as robust oxygen evolution electrocatalysts, *Adv. Mater.*, 2022, e2208904, DOI: **10.1002/adma.202208904**.

71 C.-P. Wang, H.-Y. Liu, G. Bian, X. Gao, S. Zhao, Y. Kang, J. Zhu and X.-H. Bu, Metal-layer assisted growth of ultralong quasi-2D MOF nanoarrays on arbitrary substrates for accelerated oxygen evolution, *Small*, 2019, **15**, 1906086.

72 M. Liu, L. J. Kong, X. M. Wang, J. He, J. J. Zhang, J. Zhu and X. H. Bu, Deciphering of advantageous electrocatalytic water oxidation behavior of metal-organic framework in alkaline media, *Nano Res.*, 2021, **14**, 4680–4688.

73 S. Zhao, Y. Wang, J. Dong, C.-T. He, H. Yin, P. An, K. Zhao, X. Zhang, C. Gao, L. Zhang, J. Lv, J. Wang, J. Zhang, A. M. Khattak, N. A. Khan, Z. Wei, J. Zhang, S. Liu, H. Zhao and Z. Tang, Ultrathin metal-organic framework nanosheets for electrocatalytic oxygen evolution, *Nat. Energy*, 2016, **1**, 16184.

74 S. Kandambeth, V. S. Kale, D. Fan, J. A. Bau, P. M. Bhatt, S. Zhou, A. Shkurenko, M. Rueping, G. Maurin, O. Shekhah and M. Eddaoudi, Unveiling chemically robust bimetallic squarate-based metal-organic frameworks for electrocatalytic oxygen evolution reaction, *Adv. Energy Mater.*, 2022, 2202964.

75 C.-P. Wang, Y. Feng, H. Sun, Y. Wang, J. Yin, Z. Yao, X.-H. Bu and J. Zhu, Self-optimized metal-organic framework electrocatalysts with structural stability and high current tolerance for water oxidation, *ACS Catal.*, 2021, **11**, 7132–7143.

76 M. Jahan, Z. Liu and K. P. Loh, A graphene oxide and copper-centered metal organic Framework composite as a tri-functional catalyst for HER, OER, and ORR, *Adv. Funct. Mater.*, 2013, **23**, 5363–5372.

77 Y. Wang, B. Liu, X. Shen, H. Arandiyan, T. Zhao, Y. Li, M. Garbrecht, Z. Su, L. Han, A. Tricoli and C. Zhao, Engineering the activity and stability of MOF-nanocomposites for efficient water oxidation, *Adv. Energy Mater.*, 2021, **11**, 2003759.

78 L. Zhao, B. Dong, S. Li, L. Zhou, L. Lai, Z. Wang, S. Zhao, M. Han, K. Gao, M. Lu, X. Xie, B. Chen, Z. Liu, X. Wang, H. Zhang, H. Li, J. Liu, H. Zhang, X. Huang and W. Huang, Interdiffusion reaction-assisted hybridization of two-dimensional metal-organic frameworks and $Ti_3C_2T_x$ nanosheets for electrocatalytic exygen evolution, *ACS Nano*, 2017, **11**, 5800–5807.

79 Z. Gao, Y. Lai, L. Gong, L. Zhang, S. Xi, J. Sun, L. Zhang and F. Luo, Robust Th-MOF-supported semirigid single-metal-site catalyst for an efficient acidic oxygen evolution reaction, *ACS Catal.*, 2022, **12**, 9101–9113.

80 W. Zhang, Y. Wang, H. Zheng, R. Li, Y. Tang, B. Li, C. Zhu, L. You, M. R. Gao, Z. Liu, S. H. Yu and K. Zhou, Embedding ultrafine metal oxide nanoparticles in monolayered metal-organic framework nanosheets enables efficient electrocatalytic oxygen evolution, *ACS Nano*, 2020, **14**, 1971–1981.

81 L. Zhang, J. Wang, K. Jiang, Z. Xiao, Y. Gao, S. Lin and B. Chen, Self-reconstructed metal-organic framework heterojunction for switchable oxygen evolution reaction, *Angew. Chem., Int. Ed.*, 2022, e202214794.

82 M. Liu, L. Kong, X. Wang, J. He and X.-H. Bu, Engineering bimetal synergistic electrocatalysts based on metal-organic frameworks for efficient oxygen evolution, *Small*, 2019, **15**, 1903410.

83 Z. Xue, Y. Li, Y. Zhang, W. Geng, B. Jia, J. Tang, S. Bao, H.-P. Wang, Y. Fan, Z.-w. Wei, Z. Zhang, Z. Ke, G. Li and C.-Y. Su, Modulating electronic structure of metal-organic framework for efficient electrocatalytic oxygen evolution, *Adv. Energy Mater.*, 2018, **8**, 1801564.

84 M. Zhang, B. Yang, T. Yang, Y. Yang and Z. Xiang, A ferric citrate derived Fe-N-C electrocatalyst with stepwise pyrolysis for highly efficient oxygen reduction reaction, *Chin. Chem. Lett.*, 2022, **33**, 362–367.

85 Y. Q. Cui, J. X. Xu, M. L. Wang and L. H. Guan, Surface oxidation of single-walled-carbon-nanotubes with enhanced oxygen electroreduction activity and selectivity, *Chin. J. Struct. Chem.*, 2020, **40**, 533–539.

86 M. Liu, N. Li, S. Cao, X. Wang, X. Lu, L. Kong, Y. Xu and X. H. Bu, A "Pre-Constrained Metal Twins" strategy to prepare efficient dual-metal-atom catalysts for cooperative oxygen electrocatalysis, *Adv. Mater.*, 2022, **34**, 2107421.

87 J. Mao, L. Yang, P. Yu, X. Wei and L. Mao, Electrocatalytic four-electron reduction of oxygen with Copper (II)-based metal-organic frameworks, *Electrochem. Commun.*, 2012, **19**, 29–31.

88 R. Iqbal, S. Ali, G. Yasin, S. Ibraheem, M. Tabish, M. Hamza, H. Chen, H. Xu, J. Zeng and W. Zhao, A novel 2D $Co_3(HADQ)_2$ metal-organic framework as a highly active and stable electrocatalyst for acidic oxygen reduction, *Chem. Eng. J.*, 2022, **430**, 132642.

89 M. O. Cichocka, Z. Liang, D. Feng, S. Back, S. Siahrostami, X. Wang, L. Samperisi, Y. Sun, H. Xu, N. Hedin, H. Zheng, X. Zou, H. C. Zhou and Z. Huang, A porphyrinic zirconium metal-organic framework for oxygen reduction reaction: tailoring the spacing between active-sites through chain-based inorganic building units, *J. Am. Chem. Soc.*, 2020, **142**, 15386–15395.

90 M. Liu, H. Su, W. Cheng, F. Yu, Y. Li, W. Zhou, H. Zhang, X. Sun, X. Zhang, S. Wei and Q. Liu, Synergetic dual-ion centers boosting metal organic framework alloy catalysts toward efficient two electron oxygen reduction, *Small*, 2022, **18**, e2202248.

91 X. Chen, B. Shao, M.-J. Tang, X.-L. He, F.-J. Yang, Z.-P. Guo, Z. Zhang, C.-T. He, F.-P. Huang and J. Huang, Accurately metal-modulated bimetallic metal–organic frameworks as advanced trifunctional electrocatalysts, *J. Mater. Chem. A*, 2021, **9**, 14682–14690.

92 H. Yoon, S. Lee, S. Oh, H. Park, S. Choi and M. Oh, Synthesis of bimetallic conductive 2D metal–organic framework (Co_xNi_y-CAT) and its mass production: enhanced electrochemical oxygen reduction activity, *Small*, 2019, **15**, 1805232.

93 M. Jahan, Q. Bao and K. P. Loh, Electrocatalytically active graphene-porphyrin MOF composite for oxygen reduction reaction, *J. Am. Chem. Soc.*, 2012, **134**, 6707–6713.

94 W. Cheng, X. F. Lu, D. Luan and X. W. D. Lou, NiMn-based bimetal-organic framework nanosheets supported on multi-channel carbon fibers for efficient oxygen electrocatalysis, *Angew. Chem., Int. Ed.*, 2020, **59**, 18234–18239.

95 H. Zhong, K. H. Ly, M. Wang, Y. Krupskaya, X. Han, J. Zhang, J. Zhang, V. Kataev, B. Buchner, I. M. Weidinger, S. Kaskel, P. Liu, M. Chen, R. Dong and X. Feng, A phthalocyanine-based layered two-dimensional conjugated metal-organic framework as a highly efficient electrocatalyst for the oxygen reduction reaction, *Angew. Chem., Int. Ed.*, 2019, **58**, 10677–10682.

96 X. Zheng, Y. Cao, D. Liu, M. Cai, J. Ding, X. Liu, J. Wang, W. Hu and C. Zhong, Bimetallic metal-organic-framework/reduced graphene oxide composites as bifunctional electrocatalysts for rechargeable Zn-air batteries, *ACS Appl. Mater. Interfaces*, 2019, **11**, 15662–15669.

97 K. Cho, S. H. Han and M. P. Suh, Copper-organic framework fabricated with CuS nanoparticles: synthesis, electrical conductivity, and electrocatalytic activities for oxygen reduction reaction, *Angew. Chem., Int. Ed.*, 2016, **55**, 15301–15305.

98 Z. Liang, H. Guo, G. Zhou, K. Guo, B. Wang, H. Lei, W. Zhang, H. Zheng, U. P. Apfel and R. Cao, Metal-organic-framework-supported molecular electrocatalysis for the oxygen reduction reaction, *Angew. Chem., Int. Ed.*, 2021, **60**, 8472–8476.

99 W. Cheng, X. Zhao, H. Su, F. Tang, W. Che, H. Zhang and Q. Liu, Lattice-strained metal–organic-framework arrays for bifunctional oxygen electrocatalysis, *Nat. Energy*, 2019, **4**, 115–122.

100 C. Li, M. Wang, L. Ren and H. Sun, Promoting the formation of oxygen vacancies in ceria multishelled hollow microspheres by doping iron for enhanced ambient ammonia electrosynthesis, *Inorg. Chem. Front.*, 2022, **9**, 1467–1473.

101 H. He, H.-M. Wen, H.-K. Li and H.-W. Zhang, Recent advances in metal–organic frameworks and their derivatives for electrocatalytic nitrogen reduction to ammonia, *Coord. Chem. Rev.*, 2022, **471**, 214761.

102 Y. Wang, M. Batmunkh, H. Mao, H. Li, B. Jia, S. Wu, D. Liu, X. Song, Y. Sun and T. Ma, Low-overpotential electrochemical ammonia synthesis using BiOCl-modified 2D titanium carbide MXene, *Chin. Chem. Lett.*, 2022, **33**, 394–398.

103 C. Li, Z. Qiu, H. Sun, Y. Yang and C. P. Li, Recent progress in covalent organic frameworks (COFs) for electrocatalysis, *Chin. J. Struct. Chem.*, 2022, **41**, 2211084–2211099.

104 X. Yi, X. He, F. Yin, T. Yang, B. Chen and G. Li, NH_2–MIL-88B–Fe for electrocatalytic N_2 fixation to NH_3 with high Faradaic efficiency under ambient conditions in neutral electrolyte, *J. Mater. Sci.*, 2020, **55**, 12041–12052.

105 Y. Cao, P. Li, T. Wu, M. Liu and Y. Zhang, Electrocatalysis of N_2 to NH_3 by HKUST-1 with high NH_3 yield, *Chem. – Asian J.*, 2020, **15**, 1272–1276.

106 H. He, H.-K. Li, Q.-Q. Zhu, C.-P. Li, Z. Zhang and M. Du, Hydrophobicity modulation on a ferriporphyrin-based metal–organic framework for enhanced ambient electrocatalytic nitrogen fixation, *Appl. Catal., B*, 2022, **316**, 121673.

107 J. Duan, Y. Sun, S. Chen, X. Chen and C. Zhao, A zero-dimensional nickel, iron–metal–organic framework (MOF) for synergistic N_2 electrofixation, *J. Mater. Chem. A*, 2020, **8**, 18810–18815.

108 W. Li, W. Fang, C. Wu, K. N. Dinh, H. Ren, L. Zhao, C. Liu and Q. Yan, Bimetal–MOF nanosheets as efficient bifunctional electrocatalysts for oxygen evolution and nitrogen reduction reaction, *J. Mater. Chem. A*, 2020, **8**, 3658–3666.

109 X. Liang, X. Ren, Q. Yang, L. Gao, M. Gao, Y. Yang, H. Zhu, G. Li, T. Ma and A. Liu, A two-dimensional MXene-supported metal-organic framework for highly selective ambient electrocatalytic nitrogen reduction, *Nanoscale*, 2021, **13**, 2843–2848.

110 Y. Lv, Y. Wang, M. Yang, Z. Mu, S. Liu, W. Ding and M. Ding, Nitrogen reduction through confined electro-catalysis with carbon nanotube inserted metal–organic frameworks, *J. Mater. Chem. A*, 2021, **9**, 1480–1486.

111 W.-Y. Xu, C. Li, F.-L. Li, J.-Y. Xue, W. Zhang, H. Gu, B. F. Abrahams and J.-P. Lang, A hybrid catalyst for efficient electrochemical N_2 fixation formed by decorating amorphous MoS_3 nanosheets with MIL-101(Fe) nanodots, *Sci. China: Chem.*, 2022, **65**, 885–891.

112 H. He, Q.-Q. Zhu, Y. Yan, H.-W. Zhang, Z.-Y. Han, H. Sun, J. Chen, C.-P. Li, Z. Zhang and M. Du, Metal–organic framework supported Au nanoparticles with organosilicone coating for high-efficiency electrocatalytic N_2 reduction to NH_3, *Appl. Catal., B*, 2022, **302**, 120840.

113 Y. Yang, S. Q. Wang, H. Wen, T. Ye, J. Chen, C. P. Li and M. Du, Nanoporous gold embedded ZIF composite for enhanced electrochemical nitrogen fixation, *Angew. Chem., Int. Ed.*, 2019, **58**, 15362–15366.

114 X. Zhao, F. Yin, N. Liu, G. Li, T. Fan and B. Chen, Highly efficient metal–organic-framework catalysts for electrochemical synthesis of ammonia from N_2 (air) and water at low temperature and ambient pressure, *J. Mater. Sci.*, 2017, **52**, 10175–10185.

115 X. He, F. Yin, X. Yi, T. Yang, B. Chen, X. Wu, S. Guo, G. Li and Z. Li, Defective UiO-66-NH_2 functionalized with stable superoxide radicals toward electrocatalytic nitrogen reduction with high Faradaic efficiency, *ACS Appl. Mater. Interfaces*, 2022, **14**, 26571–26586.

116 Y. Sun, B. Xia, S. Ding, L. Yu, S. Chen and J. Duan, Rigid two-dimensional indium metal–organic frameworks boosting nitrogen electroreduction at all pH values, *J. Mater. Chem. A*, 2021, **9**, 20040–20047.